1989

Development of a flight test methodology for a U.S. Navy half-scale unmanned air vehicle.

Tanner, James Christopher

Monterey, California. Naval Postgraduate School

NAVAL POSTGRADUATE SCHOOL
Monterey, California

THESIS

DEVELOPMENT OF A FLIGHT TEST METHODOLOGY
FOR A U.S. NAVY HALF-SCALE
UNMANNED AIR VEHICLE

by

James Christopher Tanner

March 1989

Thesis Advisor: Richard Howard

REPORT DOCUMENTATION PAGE

REPORT SECURITY CLASSIFICATION UNCLASSIFIED	1b RESTRICTIVE MARKINGS
SECURITY CLASSIFICATION AUTHORITY	3 DISTRIBUTION/AVAILABILITY OF REPORT APPROVED FOR PUBLIC RELEASE; DISTRIBUTION IS UNLIMITED.
DECLASSIFICATION/DOWNGRADING SCHEDULE	
PERFORMING ORGANIZATION REPORT NUMBER(S)	5 MONITORING ORGANIZATION REPORT NUMBER(S)
NAME OF PERFORMING ORGANIZATION NAVAL POSTGRADUATE SCHOOL	6b OFFICE SYMBOL (If applicable) 67
7a NAME OF MONITORING ORGANIZATION NAVAL POSTGRADUATE SCHOOL	
ADDRESS (City, State, and ZIP Code) MONTEREY, CA 93940-5000	7b ADDRESS (City, State, and ZIP Code) MONTEREY, CA 93940-5000
NAME OF FUNDING/SPONSORING ORGANIZATION	8b OFFICE SYMBOL (If applicable)
9 PROCUREMENT INSTRUMENT IDENTIFICATION NUMBER	
ADDRESS (City, State, and ZIP Code)	10 SOURCE OF FUNDING NUMBERS

PROGRAM ELEMENT NO.	PROJECT NO	TASK NO	WORK UNIT ACCESSION NO

TITLE (Include Security Classification)
DEVELOPMENT OF A FLIGHT TEST METHODOLOGY FOR A U.S. NAVY HALF-SCALE UNMANNED AIR VEHICLE

PERSONAL AUTHOR(S)
ANNER, JAMES CHRISTOPHER

TYPE OF REPORT	13b TIME COVERED	14 DATE OF REPORT (Year, Month, Day)	15 PAGE COUNT
ASTER'S THESIS	FROM _____ TO _____	1989, MARCH	107

SUPPLEMENTARY NOTATION THE VIEWS EXPRESSED IN THIS THESIS ARE THOSE OF THE AUTHOR AND DO NOT REFLECT THE OFFICIAL POLICY OR POSITION OF THE DEPARTMENT OF DEFENSE OR THE U.S. GOVERNMENT.

COSATI CODES			18 SUBJECT TERMS (Continue on reverse if necessary and identify by block number)
FIELD	GROUP	SUB-GROUP	FLIGHT TEST, UAV, RPV, PERFORMANCE, DRAG POLAR, PROPULSIVE EFFICIENCY, TORQUE STAND

ABSTRACT (Continue on reverse if necessary and identify by block number)

The development of a flight test methodology for predicting the performance characteristics of a half-scale Unmanned Air Vehicle (UAV) is discussed. This methodology is the first step in developing a UAV flight test program which will ultimately be used to help improve and/or validate the performance characteristics of these type of vehicles, currently being integrated into the U.S. Navy. The methodology determined powerplant characteristics through torque stand tests and aerodynamic characteristics through wind tunnel and flight tests. The data from these tests were used to construct power required and drag polar curves. These curves were then used to predict the basic performance characteristics of the half-scale Pioneer. The

20 DISTRIBUTION/AVAILABILITY OF ABSTRACT ☒ UNCLASSIFIED/UNLIMITED ☐ SAME AS RPT ☐ DTIC USERS	21 ABSTRACT SECURITY CLASSIFICATION UNCLASSIFIED
22a NAME OF RESPONSIBLE INDIVIDUAL CHARD HOWARD	22b TELEPHONE (Include Area Code) (408)646-2870
	22c OFFICE SYMBOL CODE 67 Ho

FORM 1473, 84 MAR 83 APR edition may be used until exhausted
All other editions are obsolete

SECURITY CLASSIFICATION OF THIS PAGE
UNCLASSIFIED

☆ U.S. Government Printing Office 1988—606-24.

Item #19 Continued:

results appear reasonable for the type of aircraft tested, within the constraints of the limited instrumentation available at this stage in the program development. The next step in the program is to use this methodology to conduct further testing in order to develop a solid data base.

Approved for public release; distribution is unlimited.

DEVELOPMENT OF A FLIGHT TEST METHODOLOGY FOR A U.S. NAVY HALF-SCALE UNMANNED AIR VEHICLE

by

James Christopher Tanner
Lieutenant, United States Navy
B.S., United States Naval Academy, 1981

Submitted in partial fulfillment of the
requirements for the degree of

MASTER OF SCIENCE IN AERONAUTICAL ENGINEERING

from the

NAVAL POSTGRADUATE SCHOOL
March 1989

ABSTRACT

The development of a flight test methodology for predicting the performance characteristics of a half-scale Unmanned Air Vehicle (UAV) is discussed. This methodology is the first step in developing a UAV flight test program which will ultimately be used to help improve and/or validate the performance characteristics of these type of vehicles, currently being integrated into the U.S. Navy. The methodology determined powerplant characteristics through torque stand tests and aerodynamic characteristics through wind tunnel and flight tests. The data from these tests were used to construct power required and drag polar curves. These curves were then used to predict the basic performance characteristics of the half-scale Pioneer. The results appear reasonable for the type of aircraft tested, within the constraints of the limited instrumentation available at this stage in the program development. The next step in the program is to use this methodology to conduct further testing in order to develop a solid data base.

TABLE OF CONTENTS

LIST OF FIGURES

TABLE OF SYMBOLS

A	Slope Coefficient for $P_{iw}V_{iw}$ Linear Regression
AR	Aspect Ratio
B	Y-Intercept Coefficient for $P_{iw}V_{iw}$ Linear Regression
C_D	Drag Coefficient
C_{Di}	Induced Drag Coefficient
C_{Do}	Parasitic Drag Coefficient
C_L	Lift Coefficient
C_{TE}	Effective Thrust Coefficient
D	Drag
ΔD	Drag Due to Action of Propeller
D	Propeller Diameter
e	Oswald Efficiency Factor
F	Torque Stand Force
F	Wind Tunnel Calibration Factor
f	Propeller Frequency
J	Advance Ratio
L	Aircraft Lift
l	Torque Arm Length
n	Propeller Revolution
P	Aircraft Power
P_{iw}	Power (Corrected for standard day and standard weight)
P_R	Power Required
P_T	Test Pressure
PP_{WV}	Partial Pressure Water Vapor
Q	Torque
Q_{DMM}	DMM Readout Due to Electric Motor Torque Contribution on the Wind Tunnel Balance
q	Dynamic Pressure
R	Propeller Horizontal Force
R_{DMM}	DMM Readout of Propeller Horizontal Force (Includes Electric Motor Torque Contribution)
S	Wing Area
SBHP	Shaft Brake Horsepower
$SBHP_{ALT}$	Shaft Brake Horsepower at Altitude
$SBHP_{STD}$	Shaft Brake Horsepower Corrected for Standard Day Conditions
$SPHP_T$	Test Shaft Brake Horsepower
T	Aircraft Thrust
T_E	Effective Thrust
T_T	Test Temperature
V	Velocity
V_E	Equivalent Velocity
V_{iw}	Velocity Corrected for Standard Day, Standard Weight
V_T	True Velocity
W	Aircraft Weight

W_S	Standard Weight
W_T	Test Weight
σ	Density Ratio
ρ	Air Density
ρ_o	Sea Level Air Density
η	Propeller Efficiency

ACKNOWLEDGEMENT

First I would like to thank Pat Hickey, Don Harvey, Jack King and Jim Nageotte for sharing their technical expertise and for their part in the design and construction of the wind tunnel balance. I would also like to express my thanks to John Moulton for his repair work on the half-scale Pioneer. Special thanks to our external pilot, Don Meeks. His experience in radio controlled flight and his interest in flight test helped get this project "off the ground." I would also like to express my thanks to my thesis advisor, Dr. Richard Howard, for implementing this program and for his dedication, long hours and guidance on this project.

Most of all, I would like to thank my daughter, Katie, and my wife, Sandee, for their love, personal strength and continual support during this project.

I. INTRODUCTION

Military weapon technology has become more and more complex and expensive, especially in the area of airborne weaponry. Military aircraft technology is advancing far faster than the ability of pilots to oversee it. The increased sophistication of air-to-air and surface-to-air missiles have caused the airborne battlefield to become too hazardous, in many cases, for manned flight. A solution to this problem was demonstrated by the Israelis in June, 1982. A relatively simple squadron of Israeli-built Unmanned Air Vehicles (UAV) led the attack on a Syrian stronghold in the Bekaa Valley during the Israel-Lebanon conflict. The remotely piloted UAVs provided key decoy work and gathered reconnaissance data on surface-to-air missile sites in the valley. The UAV's emitted electronic signals that mimicked radar signals generated from Israeli jets. When the air to surface missile radar systems locked on to these signals, the UAV's identified and passed on their location and characteristic radar emissions, enabling Israeli smart missiles to destroy 29 SAM sites in an hour. Following the battle the UAV's were used for battle damage assessment and to monitor Syrian troop movement [Ref. 1:pp. 38-43].

On 4 December 1983, U.S. Navy aircraft launched an attack on Syrian positions in retaliation for earlier attacks on reconnaissance aircraft. Two aircraft were shot down, one pilot killed, one crewman captured and several civilians on the ground killed from one of the lost aircraft. As a result of the loss of the U. S. Navy aircraft over Lebanon, then Secretary of the Navy John Lehman was convinced that UAV's could have spared pilots from danger, and he set out to procure such a system for the U.S. military [Ref. 2:p. 1]. In 1986 the Pioneer was selected as the U.S. Navy and Marine Corps short-range UAV system. The procurement of a UAV system, once thought useful only as a target drone, marked the beginning of the UAV concept as an important weapon system, worthy of an increased role in U.S. military thinking [Ref. 1:p. 38].

II. SCOPE

This increased attention in the UAV concept has sparked an interest in the Department of Aeronautics and Astronautics at the Naval Postgraduate School (NPS). The relatively low cost, small size, reduced risk and inherent flexibility of an UAV will allow the department to become actively involved in research test and evaluation of these vehicles.

Anticipating the delivery of a full scale UAV similar to those currently operational in the U.S. Navy, the NPS Aeronautics and Astronautics department has established its own UAV program. One goal of the NPS UAV program is to investigate methods of improving and/or validating the performance characteristics of these vehicles. This validation is required as the current U.S. Navy UAV programs are not adhering to standard Test and Evaluation processes. Due to the urgency of obtaining a viable UAV system, current systems are being procured as "off the shelf" systems, where Test and Evaluation and operational use are being conducted concurrently. The advantage to this method is that the system is integrated into the fleet quickly. The disadvantage is that the system is not tested prior to fleet integration and subsequent problems encountered are difficult to fix.

Another goal is to use these type vehicles as research test beds for other inflight research projects in a real

flight environment. High lift devices, winglets, boundary layer control methods, and improved propeller design represent areas of interest which could easily be applied to a UAV. The use of a UAV would allow research of aerodynamic phenomena in a relatively hazard free environment at a fraction of the cost of full scale research. Another advantage to inflight testing is the capability of making dynamic measurements.

In order to study the effects of design changes on aircraft performance, or prior to using these vehicles as a test bed, the vehicle's baseline performance must first be determined. The goal of this investigation is to establish a UAV testing facility and to develop a flight testing methodology which will predict the performance characteristics of these vehicles. This goal will be accomplished using a radio controlled, half-scale version of the U.S. Navy's current short-range UAV, the Pioneer. The half-scale Pioneer will also serve as an external pilot trainer for the full scale vehicles.

III. EXPERIMENTAL EQUIPMENT

The major items used in this investigation included the flight test vehicle, low speed wind tunnel, wind tunnel model, wind tunnel balance and engine torque stand.

A. FLIGHT TEST VEHICLE

The flight test vehicle used for this investigation, shown in Figure 1, was a radio controlled, half-scale model of the

Figure 1. Half-Scale Pioneer

U. S. Navy's current short-range UAV, the Pioneer. The half-scale Pioneer is currently being used as an intermediate trainer for UAV flight school by the Navy and Marine Corps. The half-scale Pioneer is a twin tail boom, pusher type, vehicle constructed primarily of fiberglass with quarter-inch plywood bulkheads and support ribs. The half-scale Pioneer has a wing span of 8.19 feet, a chord of 0.91 feet and an aspect ratio of 9.03. The rectangular wing consists of a Clark Y airfoil with no sweep, dihedral or twist. The fuselage has a trapezoidal cross-sectional area of 0.29 square feet and is 4.17 feet in length. The twin tail booms, constructed of 1-inch aluminum tubing, are 2.67 feet long and support the elevator and twin rudders. The overall length of the aircraft is 5.92 feet. A 3-D view of the half-scale Pioneer is shown in Figure 2 and a summary of the vehicle's specifications is listed in Appendix A.

The aircraft is powered by an O. S. MAX-108 FSR two-stroke glow plug engine. The engine has a 1.088 cubic inch displacement and is rated at 3 HP at 16000 RPM. The engine RPM range is 2000 to 16000 RPM. The engine drives a 14-inch diameter, 6-inch pitch pusher (14 X 6 P) propeller. The engine fuel-to-air mixture is controlled by a needle valve located on the carburetor venturi. The engine is also equipped with a muffler to reduce engine noise.

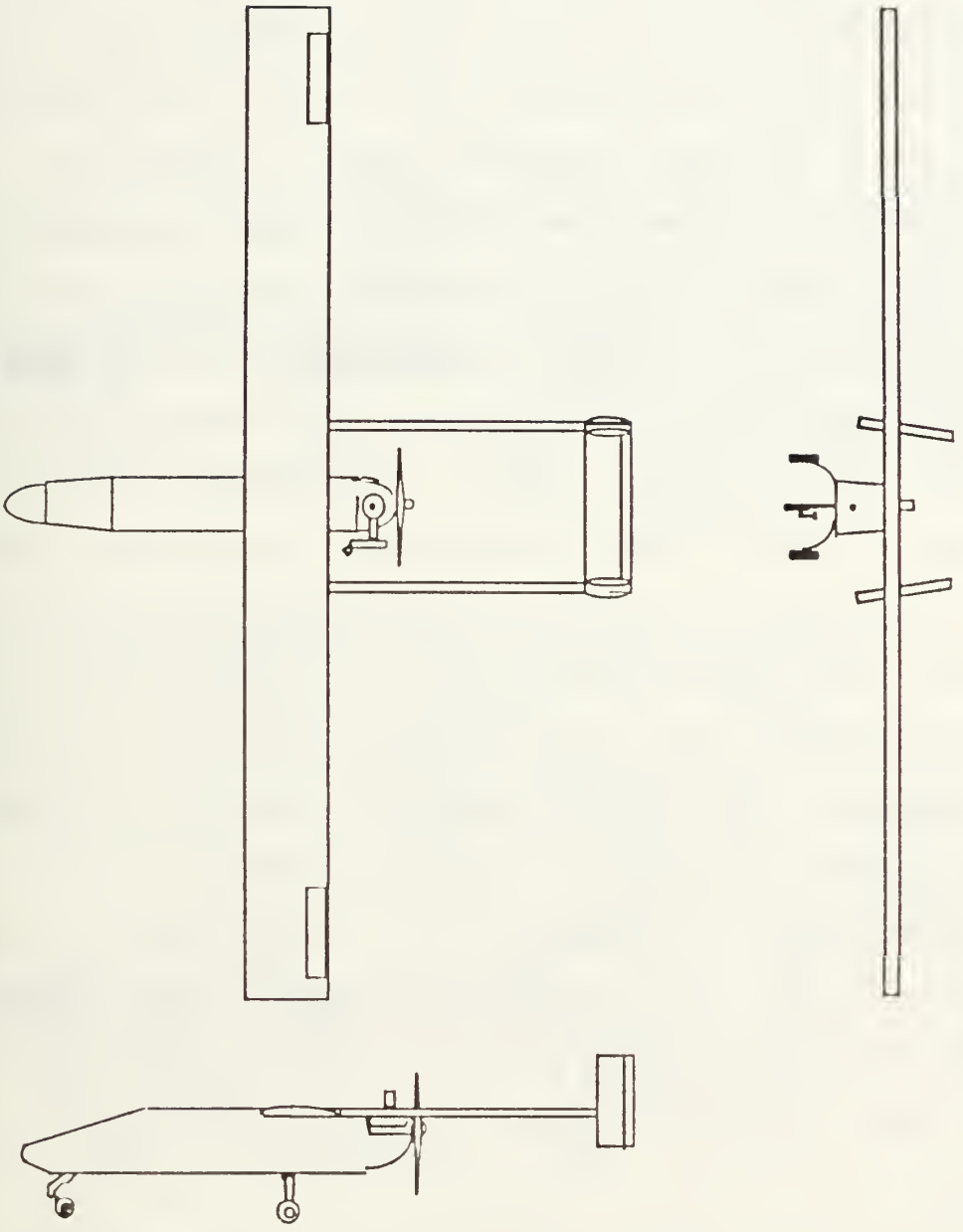

Figure 2. 3-D View of Half-Scale Pioneer

The radio control gear consisted of an eight-channel Futaba transmitter and receiver, two Futaba rate gyros, seven Futaba servos and a 4.8-volt, 1200-milliamp, Sanyo battery pack. The Futaba transmitter used a pulse coded modulated signal which provided increased signal reliability. The transmitter was also equipped with an optical tachometer wand to measure propeller RPM to ± 100 RPM. The Futaba rate gyros were mounted on the aircraft longitudinal center of gravity (CG) and were used to help stabilize the aircraft pitch and roll axes during flight testing and to lighten the pilot's workload. Figure 3 shows the electronic gear layout used in this investigation. The aircraft's control surfaces, throttle and nose wheel steering were controlled through servos. All control surface servos were mounted externally, near the surface being controlled in order to reduce the length of control surface linkages.

The suggested center of gravity (CG) was 33 percent mean aerodynamic chord (C_{MAC}). To achieve this CG position 2 pounds of additional weight were placed in the nose which put the flight test gross weight for this investigation at 27.0 pounds.

The fuel supply system consisted of an 18-ounce fuel tank, a fuselage mounted fueling connection and a Perry Regulated fuel pump. The fuel tank was mounted on the aircraft longitudinal CG so as to minimize CG movement during flight. Because the fuel tank was located approximately 15 inches

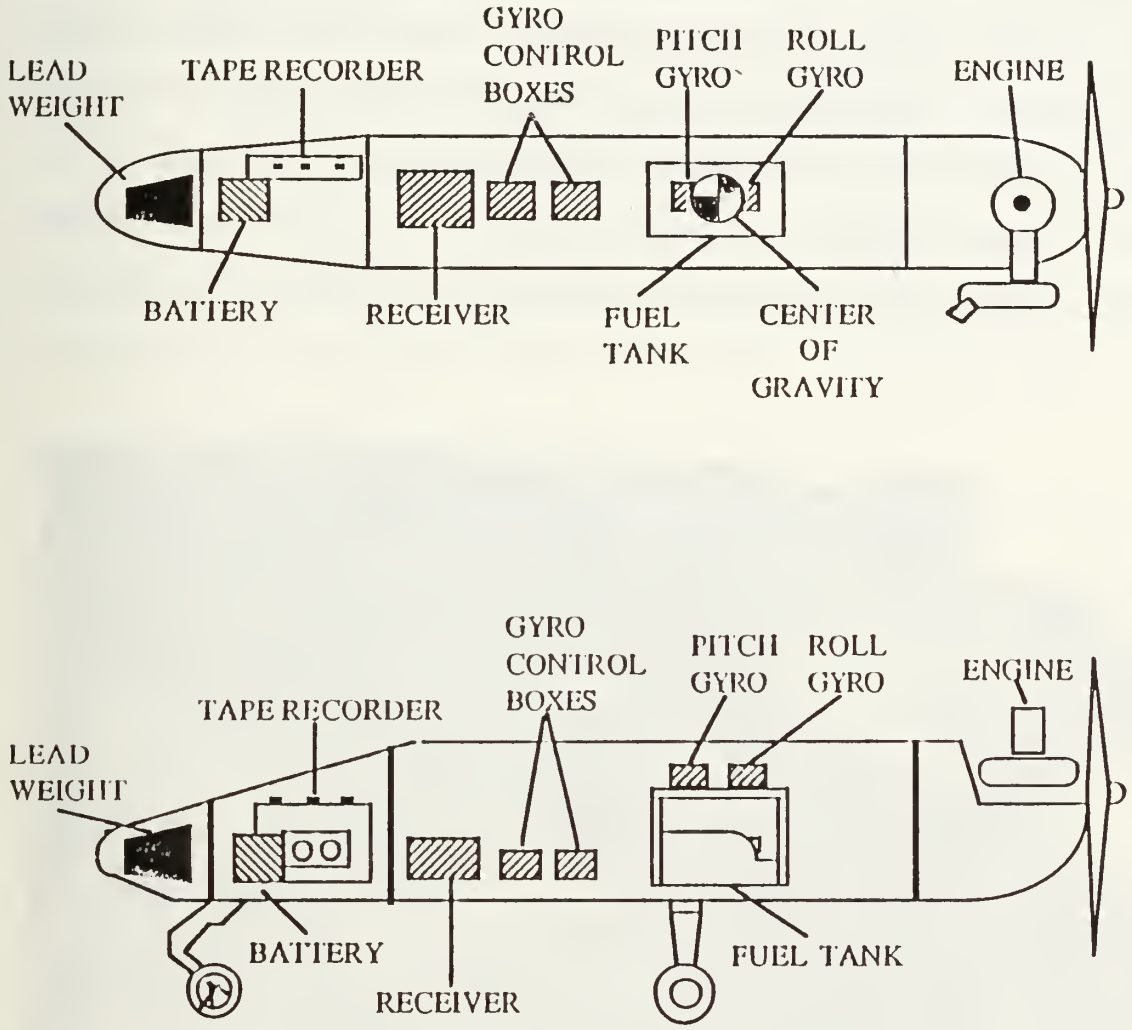

Figure 3. Half-Scale Pioneer Equipment Layout

behind and 5 inches below the engine, the fuel pump was installed to ensure a positive fuel head to the engine. The fuel system provided an endurance time of approximately 20 minutes.

A Minarik PK-1 magnetic proximity sensor was installed on the aircraft radial engine mount as shown in Figure 4. Two steel posts, 0.125 inches in diameter and 0.75 inches in length, were mounted 180 degrees apart in the engine drive washer. Once the optimum distance between the magnetic

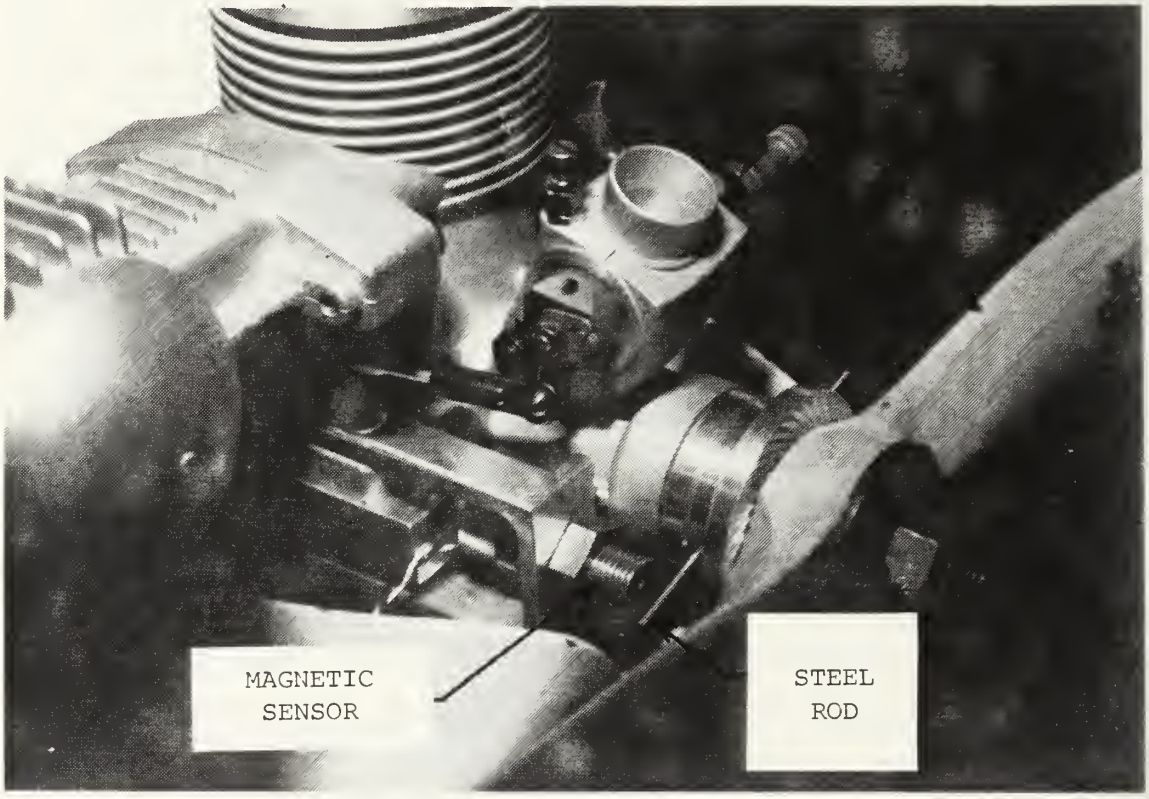

Figure 4. Inflight RPM Indication System

proximity sensor and the steel posts for the best signal was obtained, both the steel posts and the PK-1 were locked into position with permanent threadlock. The rotating steel posts passing the magnetic pickup generated a 0.5 volt sawtooth electrical signal which was recorded on an onboard tape recorder. The wiring between the tape recorder and the pick-up was shielded to ensure interference with the radio control gear would not occur. Following the flight the tape was played back into a frequency counter which enabled the calculation of the inflight engine RPM.

B. ENGINE TEST STAND

To facilitate the required engine break-in period and to test the effectiveness of different RPM indicators, a hardwood test stand was constructed and mounted on a heavy steel bench as shown in Figure 5. To minimize vibration effects rubber pads were mounted between the test stand and the bench and also between the engine and the test stand. The fuel system for the test stand consisted of the same elements as the those of the half-scale Pioneer. The fuel tank, located behind the test stand face as shown in Figure 6, was mounted on foam rubber to keep engine vibrations from foaming the fuel.

C. WIND TUNNEL

The Naval Postgraduate School low speed, vertical wind tunnel was used in this investigation. The tunnel, shown in Figure 7, is a subsonic, single return, closed circuit type.

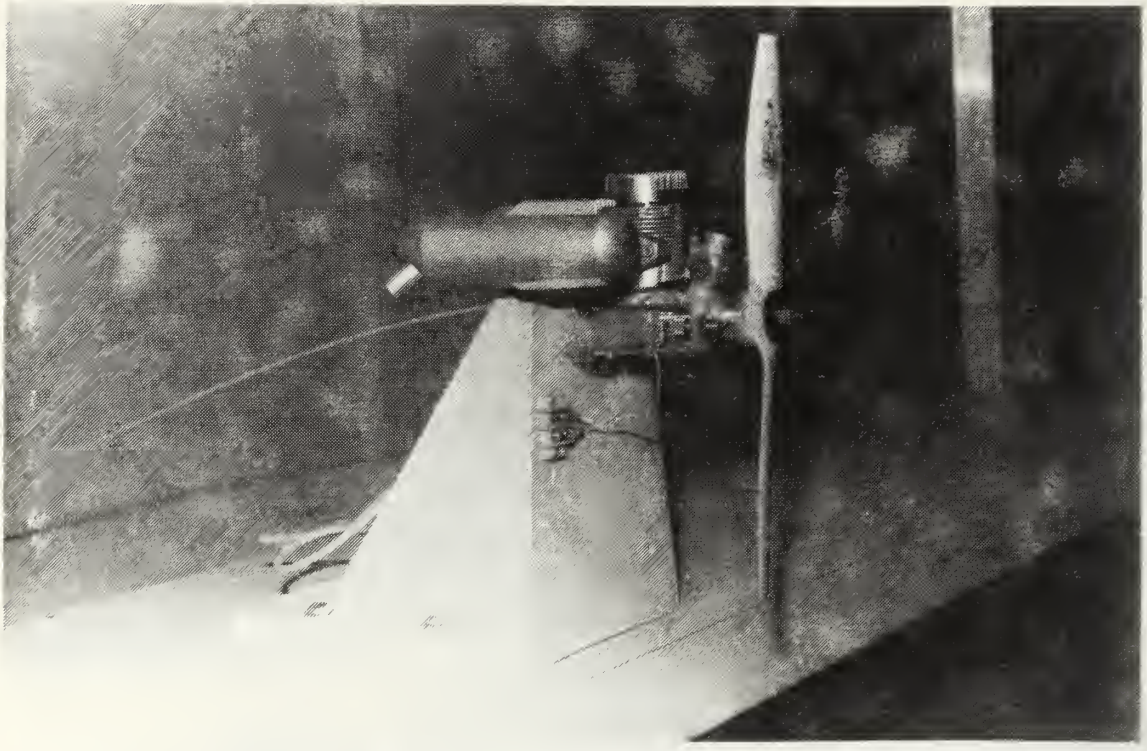

Figure 5. Engine Test Stand

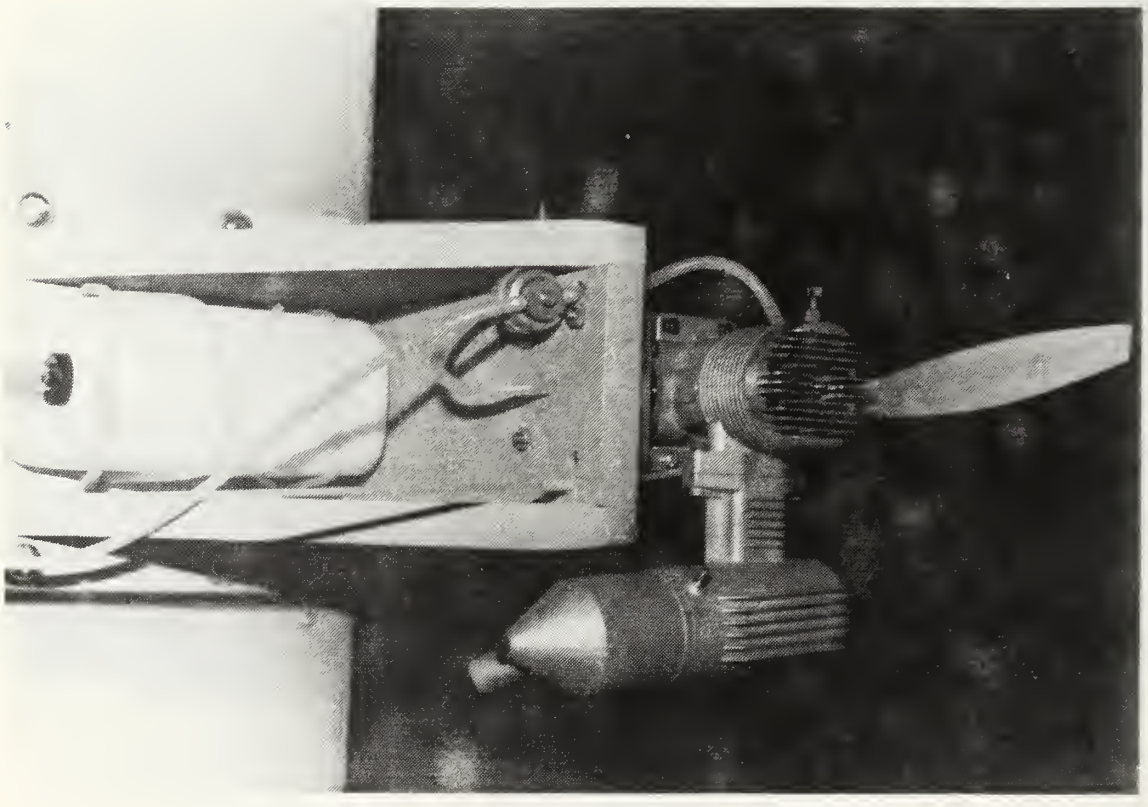

Figure 6. Engine Test Stand (Top View)

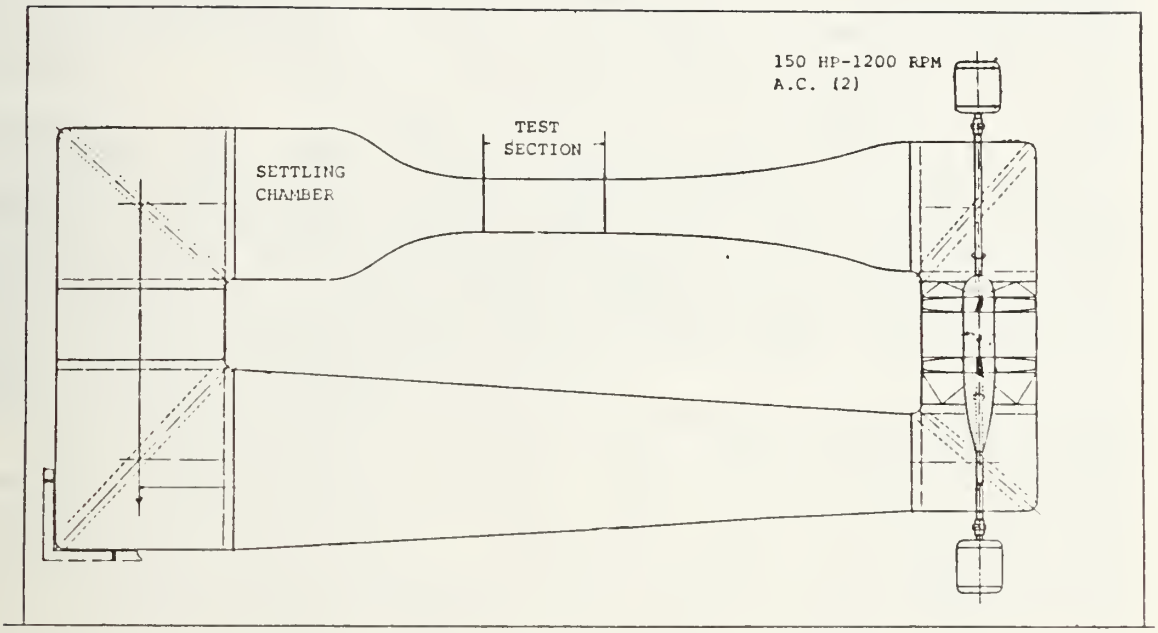

Figure 7. NPS Vertical Low Speed Wind Tunnel

The test section has a 3.5 X 5.0 foot octagon cross-section and is eight feet long. The tunnel was originally designed to operate with two sets of counter-rotating propeller blades driven by two, 150-HP AC electric motors. The top set of blades were removed and the associated engine disengaged due to blade damage. The removal of these blades decreased the wind tunnel maximum speed from approximately 300 ft/s to 200 ft/s and introduced some swirl to the flow [Ref. 3:pp. 35-36]. The wind tunnel turbulence level was 1.2 percent. Some of the swirl was removed by adjusting the turning vanes, and previous studies of the test section flow quality with one set

of blades operating showed a uniform distribution of velocity across the test section. These same studies showed that the remaining induced swirl was only a factor near the wind tunnel walls. [Ref. 4:pp. 11-12].

Two sets of static pressure port rings were used to measure tunnel speed. One ring set was located at the test section entrance and the other was located just upstream of the contraction cone. The pressure differential across the two ring sets was measured on a water micro-manometer. The pressure differential, once calibrated, corresponds to the dynamic pressure in the test section. Wind tunnel calibration and the calibration factor are discussed in Section VA.

D. WIND TUNNEL BALANCE

The wind tunnel balance for this investigation was designed by the author and machined by the school's metal shop personnel. The requirements for the balance were that it measure forces in the longitudinal direction for both tractor and pusher type configurations and serve as a model wind tunnel mount. Appendix B details the factors involved in the selection of the balance dimensions and the theory involved in the force measurement.

The balance was constructed out of aluminum and was 18.38 inches tall, 3.00 inches wide and 0.50 inches thick. A 2.25 inch by 1.50 inch "window" was cut out of the aluminum beam,

as shown in Figure 8, in order to reduce the cross-sectional area. The purpose of this "window" was twofold. The reduction provided an effective cross-sectional area small enough to allow the beam to bend while still maintaining a cross-sectional area large enough at the beam ends for mounting the model to the balance and the balance to the tunnel floor. Four 120 OHM bonded resistance strain gages were mounted in the "window" as shown in Figure 8.

The strain gages were wired into a four arm active bridge at the balance. Four strain gages were used to increase sensitivity and to provide automatic temperature compensation. A ten wire hook-up (Figure 9) from this bridge was then run through shielded cable to a Pacific Instruments, Model 8255, Transducer Amplifier. The bridge was completed at the balance in order to increase the noise damping capability of the amplifier. This amplifier provided bridge excitation, balance and amplification for the four arm strain gage set-up. The ten wire shielded input was recommended by the Pacific Amplifier manual as the best set-up for the highest accuracy, resolution and sensitivity. Two Hewlett Packard Digital Multimeters (DMM) were used to monitor the amplifier operation and output. One DMM monitored the amplifier excitation voltage and the other DMM was used to display the output voltage. Figure 10 shows a schematic drawing of the wind tunnel balance, strain gage orientation and instrumentation. The balance was statically calibrated to set the excitation voltage so that 0.01 millivolts on the DMM corresponded to 1.00 lb of horizontal force in the longitudinal direction.

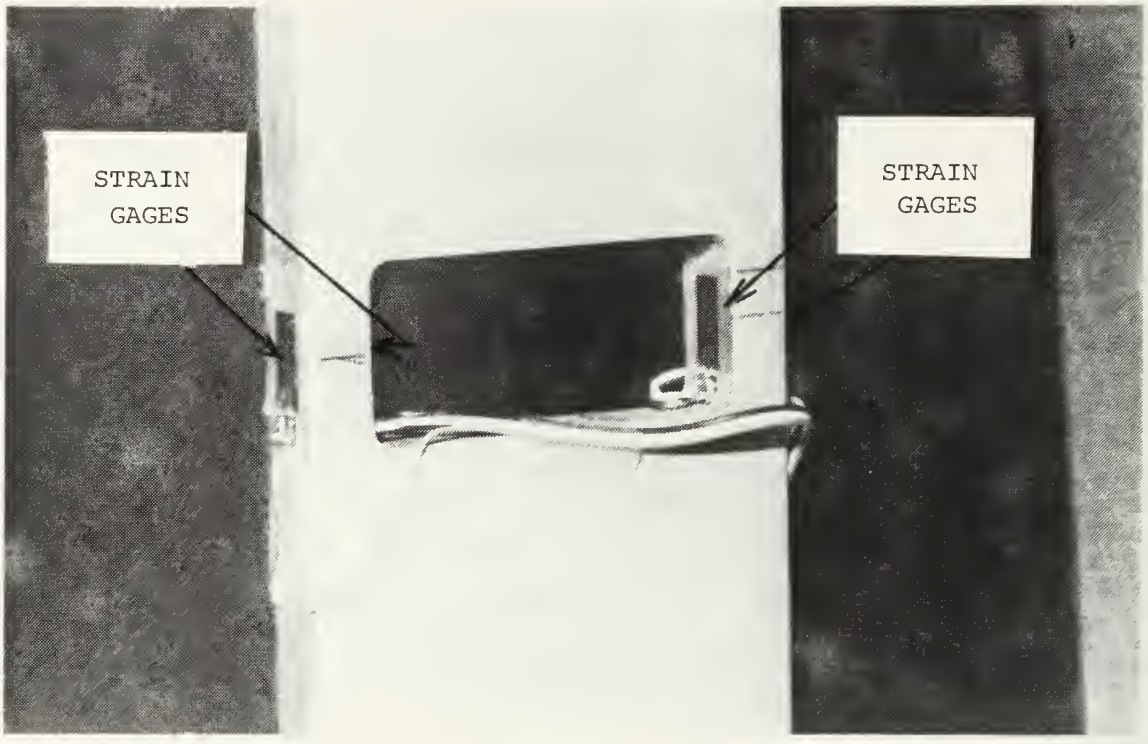

Figure 8. Wind Tunnel Balance Detail

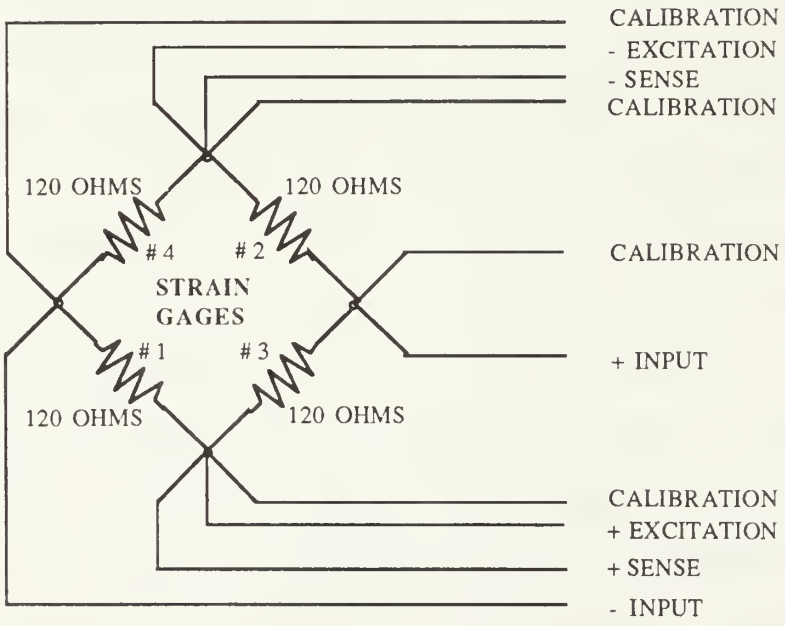

Figure 9. Wind Tunnel Balance Ten-Wire Hook-Up

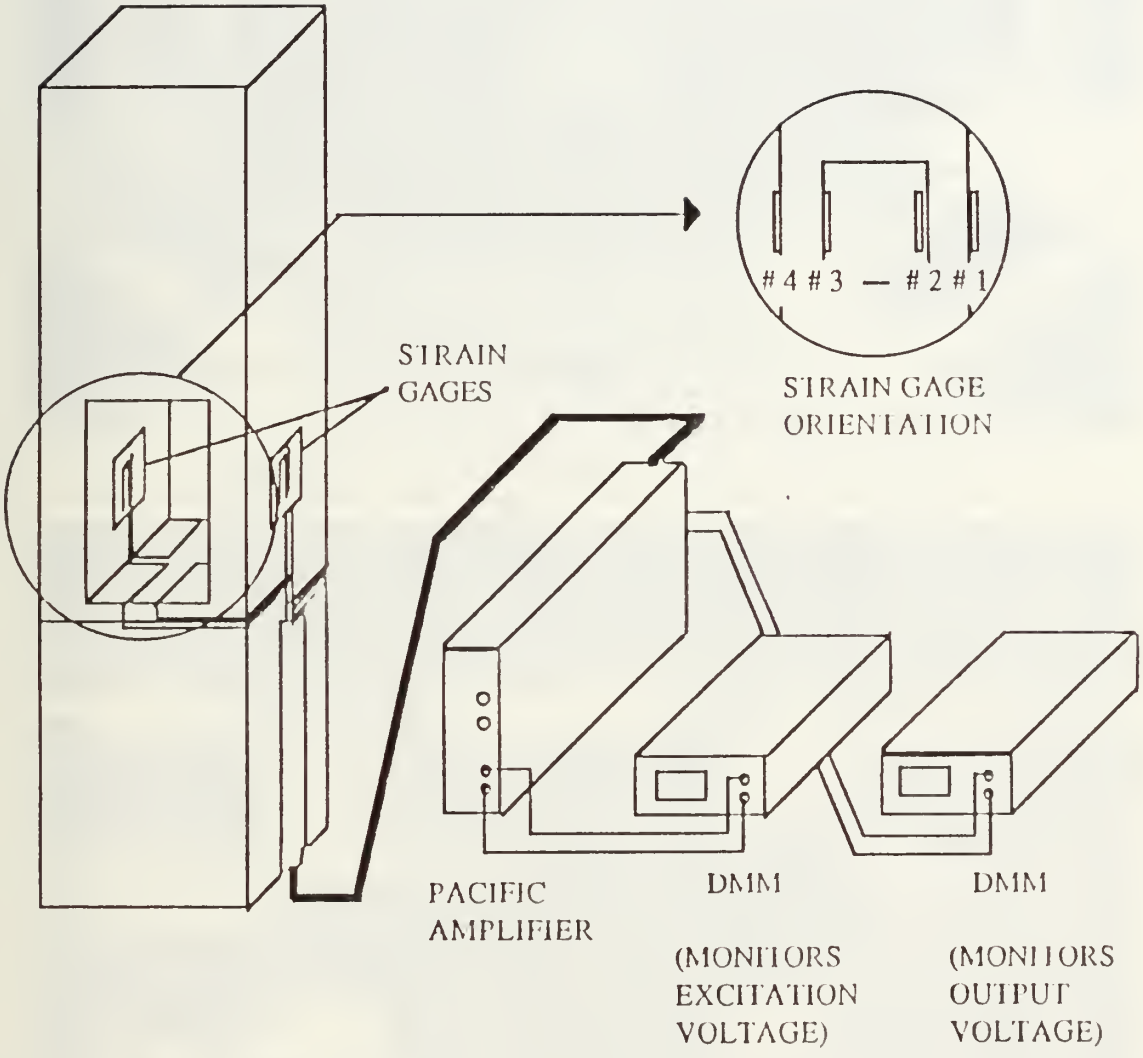

Figure 10. Wind Tunnel Balance Instrumentation Schematic

E. WIND TUNNEL MODEL

Wind tunnel testing was conducted to determine propeller efficiency. The pusher configuration of the half-scale Pioneer necessitated an accurate modeling of the airflow through the propeller disk plane. To meet this requirement great care was taken to construct a model which consisted of the components that affected the flow through the disk plane. These components for this investigation were the fuselage, wing and engine. The fuselage was constructed out of fiberglass and had the same cross-sectional size and shape but was shortened to accommodate the wind tunnel balance. The wings were constructed by covering a foam replica of the wing with fiberglass. Because only a small portion of the wing affects the flow through the propeller disk plane and to accommodate the wind tunnel test section dimensions, the wing span was shortened to three feet. Since an electric motor was used as the model powerplant, the half-scale Pioneer engine had to be modeled to obtain the proper blockage. A wooden cylinder head and the actual engine muffler were securely attached to the model in the same relative position as on the test vehicle. Figures 11 and 12 show the model as it was mounted in the wind tunnel test section.

The engine used to turn the propeller on the wind tunnel model was an AC/DC reversible motor. An electric motor was chosen over the actual engine for several reasons. The running of an internal combustion engine in a closed wind

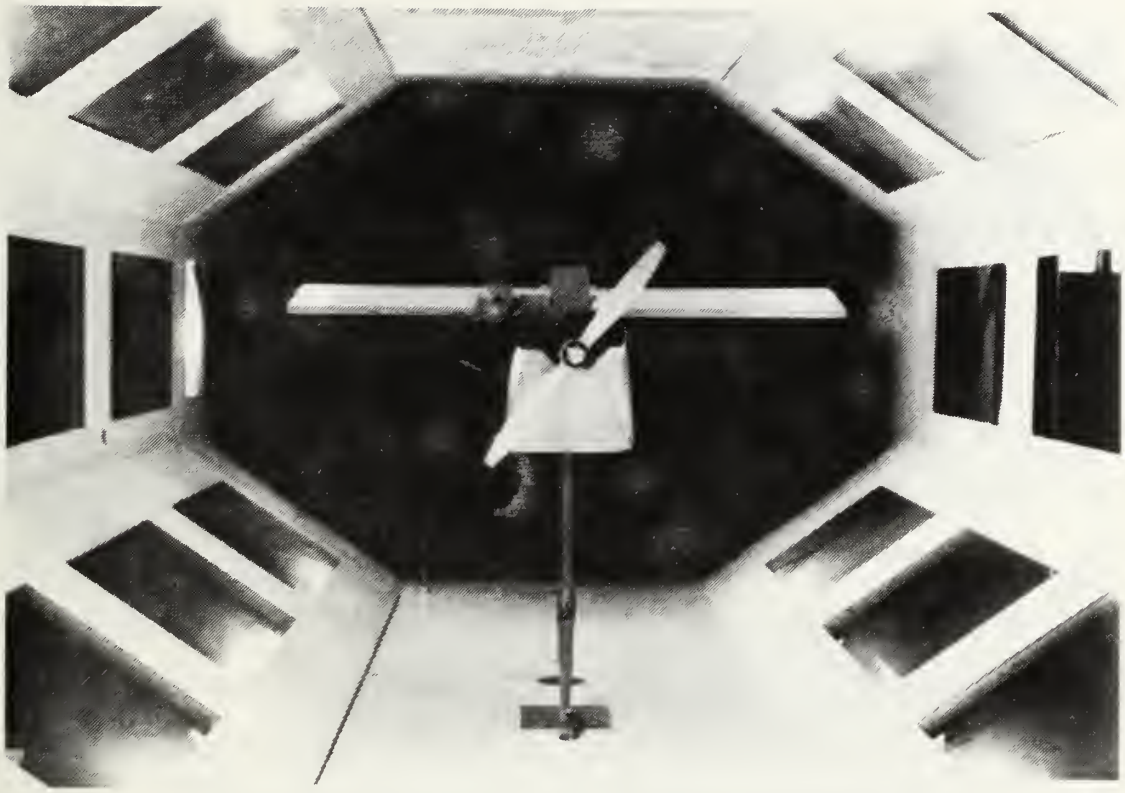

Figure 11. Wind Tunnel Model (Aft View)

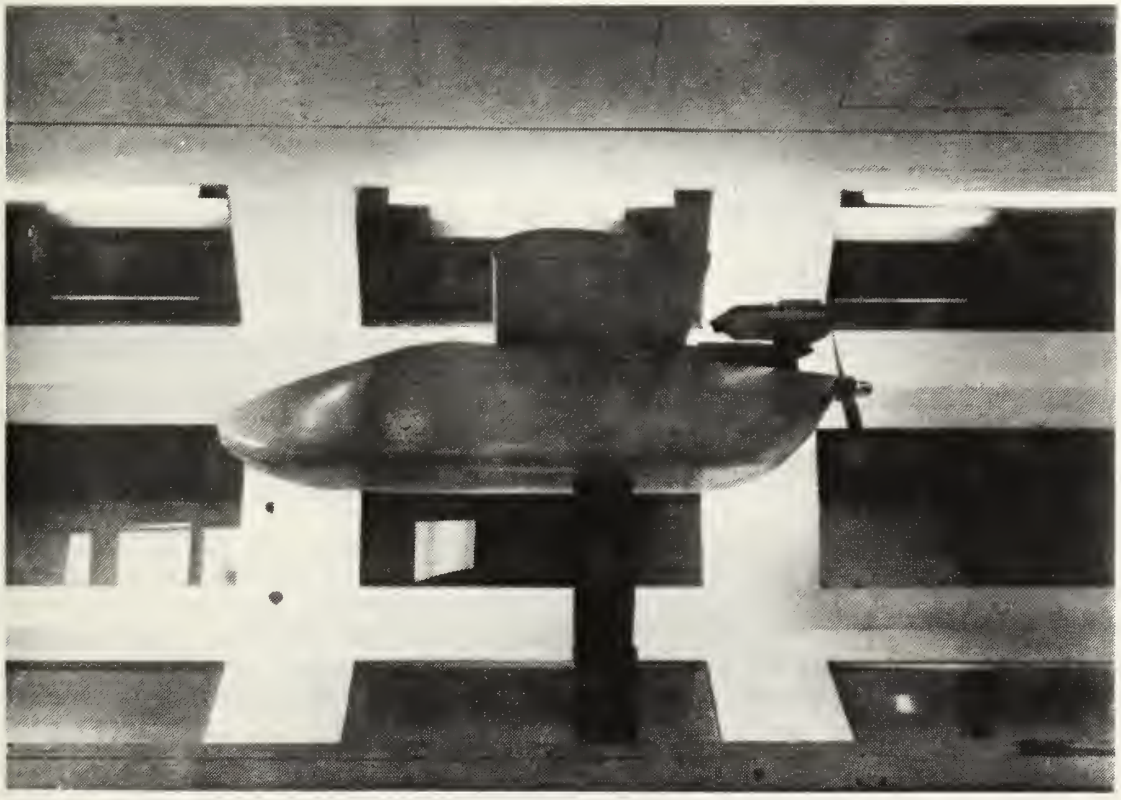

Figure 12. Wind Tunnel Model (Side View)

tunnel results in pollution problems on the tunnel walls from engine exhaust and requires purging of the tunnel. Safety considerations were also a factor. Starting a glow plug engine with a hand held starter in a small space and the presence of fuel in a wooden tunnel were determined to be hazardous operations. Engine control and fuel supply limitations were also problems. The use of an electric engine would eliminate these problems, would be easier to control and would run with less vibration.

Propeller RPM was controlled by varying the input voltage to the electric motor through a variable transformer. The transformer was capable of varying the voltage from 0 to 140 volts. The propeller drive shaft was equipped with a 30 tooth pick-up wheel and a non-contact magnetic transducer was mounted on the model as shown in Figure 13. The mechanical motion of the rotating pick-up wheel as it passed the magnetic proximity switch generated a 0.5 volt sawtooth electrical signal. This signal was sent to a Minarik VT-3 Digital Tachometer which converted the signal to RPM. The gate time for the RPM was set at 2 seconds.

F. TORQUE STAND

An engine torque stand was used to collect electrical motor and half-scale Pioneer engine torque data. The torque stand was constructed out of aluminum and mounted on a heavy steel bench. The torque stand consisted of an engine mount

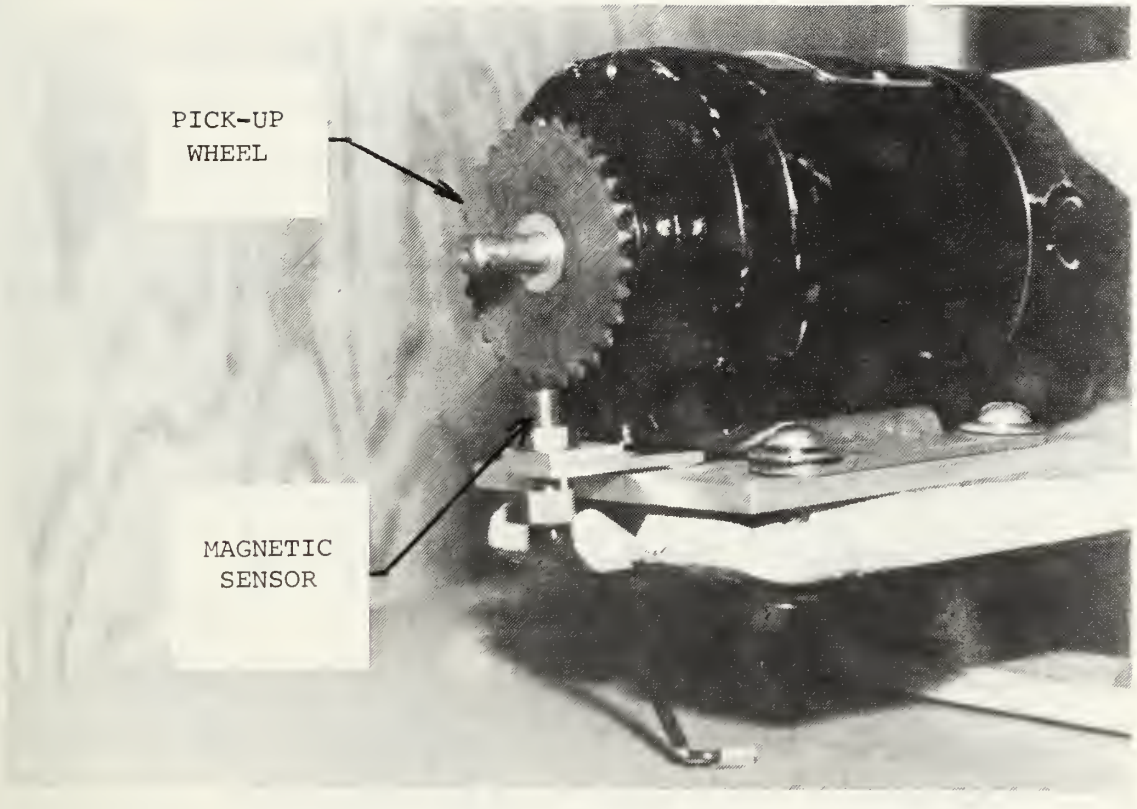

Figure 13. Wind Tunnel Model RPM Indication System

face plate, shaft, shaft housing, torque arm and a scale. Figure 14 illustrates the basic torque stand parts. The engine mount face plate was attached to a shaft which was supported by two thrust bearings. The thrust bearings were mounted in the shaft housing assembly which was securely mounted to the bench. This design allowed the engine mount face plate to rotate freely with the shaft. A 2-foot torque arm was attached to the face plate on one end and the other end rested on the scale. The force generated by the propeller-engine action-reaction, acted to rotate the face plate. This rotation was transferred through the torque arm

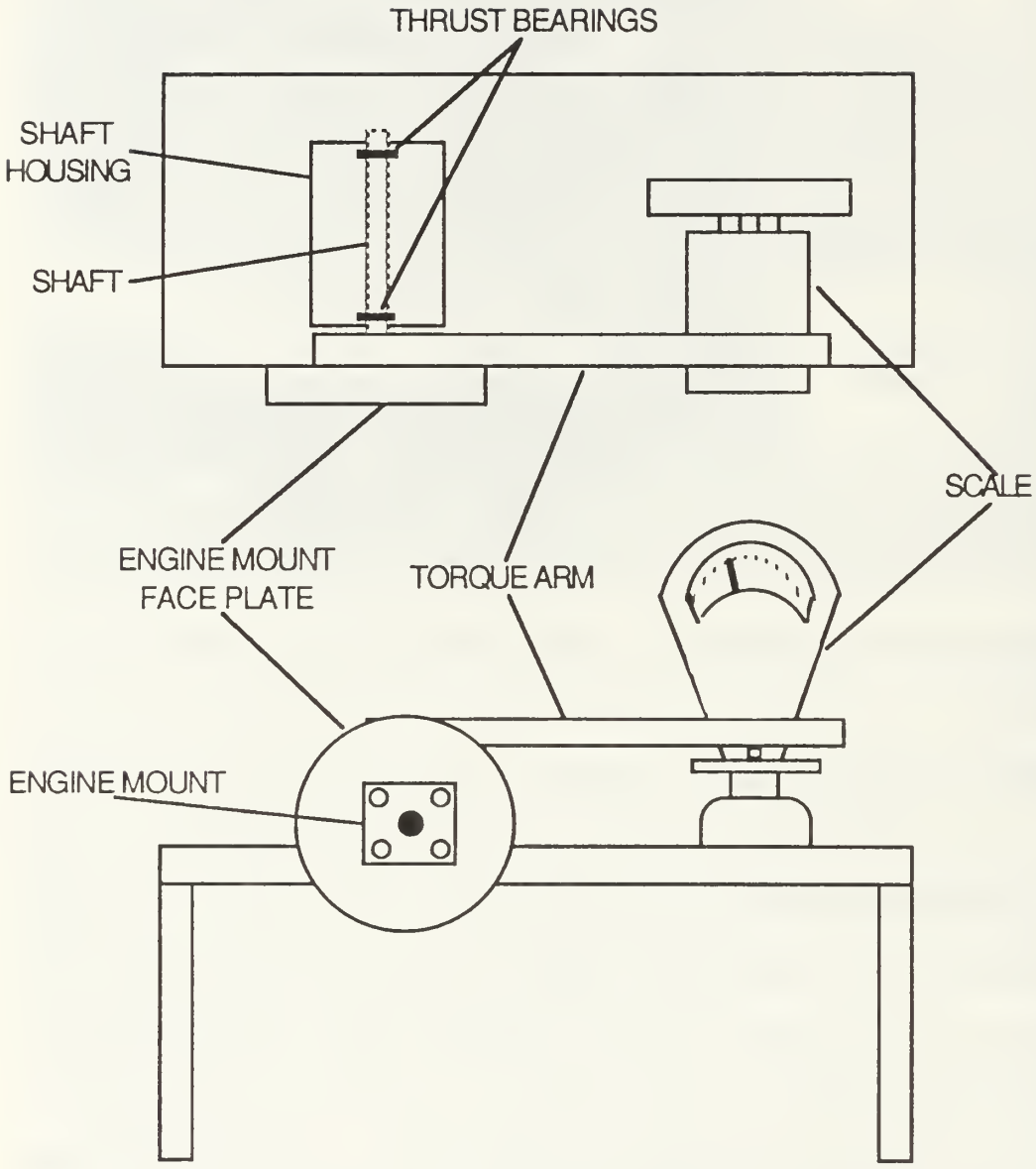

Figure 14. Engine Torque Stand

to the scale where the generated rotational force could be measured. Plywood shielding (not shown) protected the torque arm and scale from the effects of the prop wash.

Both the electric motor and the engine were tested on the torque stand. RPM control and RPM measurement for the electric motor were conducted in the same manner as the wind tunnel test. RPM control for the engine was accomplished using the transmitter, receiver, battery pack and throttle servo discussed in the flight test vehicle section. These components were securely attached to the test bench. The throttle servo for the torque stand was oriented in the same relative position as the flight test vehicle servo so throttle settings for the torque stand and the vehicle would be identical. RPM measurements were conducted on the torque stand with the same apparatus as that on the flight test vehicle, except the RPM signal was sent to the digital tachometer instead of the tape recorder. The digital tachometer had the capability to program the number of teeth passing the magnetic sensor in one revolution. The tachometer was set for two teeth per revolution and gate time was set for 3 seconds.

The fuel system components for the torque stand engine tests were identical to the flight test vehicle components. The same length fuel lines between the components and their relative position on the flight test vehicle were maintained to ensure engine operating conditions were the same.

IV. THEORY

Aircraft performance is a function of aircraft and powerplant characteristics. The aerodynamic characteristics of the aircraft define the power required and the powerplant defines the power available. A good combination between aerodynamic and powerplant characteristics is an essential element in an aircraft's ability to best perform its mission [Ref. 5:p. 5.3]. In order to analyze aircraft performance a methodology to determine the aerodynamic and powerplant characteristics must be developed.

Inflight testing to determine aircraft performance is desired because the testing is done under actual conditions and corrections are minimized. However, means to accurately measure the propeller thrust and the engine power inflight are not feasible for a minimally instrumented UAV. It was therefore necessary to use wind tunnel tests to determine propeller efficiency and torque stand tests to measure the engine shaft brake horsepower (SBHP). This information along with inflight engine RPM and velocity data will allow construction of drag polar and power required plots. From these plots the basic aerodynamic characteristics can be determined for the given aircraft configuration.

The theory for this investigation was broken into three sections related to the three phases of experimentation. The

first phase measured powerplant SBHP versus RPM using an engine torque stand. The second phase measured propeller efficiency using propulsive thrust, velocity and RPM data from wind tunnel tests and motor SBHP and RPM data from the engine torque stand tests. The third phase consisted of flight tests which determined the inflight RPM versus aircraft velocity and used the propeller efficiency data and powerplant data to construct drag polar and power required plots.

A. POWERPLANT CHARACTERISTICS

A torque stand is a relatively simple device for measuring the torque reaction from an operating engine. The torque developed by the engine-propeller action-reaction is transferred along the torque arm. The force (F) at the end of the arm is measured and the torque (Q) can be computed from the following equation:

$$Q = Fl \tag{1}$$

where l is the distance measured from the engine axis of rotation to the application point of the force measurement [Ref. 6:p. 25]. The test shaft brake horsepower ($SBHP_T$) can then be calculated:

$$SBHP_T = \frac{2\pi nQ}{550} \tag{2}$$

where n is the propeller revolutions per second (RPS) [Ref 6: p. 26].

To standardize the data for air breathing engines, the $SBHP_T$ must be corrected to standard day sea level conditions:

$$SBHP_{STD} = SBHP_T \left(\frac{29.92}{P_T - PP_{WV}}\right)\left(\frac{T_T}{518.6}\right)^{1/2} \quad (3)$$

where P_T is the test condition barometric pressure, T_T is the test condition atmospheric temperature and PP_{WV} is the water vapor partial pressure [Ref. 6: p. 26].

B. PROPULSIVE EFFICIENCY

The propeller efficiency required for this investigation is termed propulsive efficiency (η). It is the most useful way of expressing efficiency because it evaluates only the net thrust which the propeller develops when acting on a given installation. It is this efficiency which relates the power delivered to the propeller by the engine and the power required to power the aircraft [Ref. 7:p. 28]:

$$P_R = \eta SBHP_{STD} \quad (4)$$

Propulsive efficiency (η) is defined as:

$$\eta = \frac{T_E V}{P} \quad (5)$$

where T_E is the effective thrust, V is the free stream velocity and P is the $SBHP_{STD}$ of the engine [Ref. 8:p. 625]. T_E is defined as:

$$T_E = T - \Delta D \quad (6)$$

and the propeller horizontal thrust (R) for a turning propeller is defined as:

$$R = T - D - \Delta D \quad (7)$$

where T is the thrust of the propeller operating in the presence of a body, D is the drag with the propeller removed at the same free stream velocity and angle of attack and ΔD is the increase in drag due to the action of the propeller. The ΔD term includes the profile drag, induced drag due to lifting surfaces in the system and jet boundary interference drag due to testing in a wind tunnel [Ref. 8:p. 629]. Rearranging Equation 7 and substituting into Equation 6 gives:

$$T_E = R+D \tag{8}$$

Propulsive efficiency can then be written as:

$$\eta = \frac{(R+D)V}{P} \tag{9}$$

In order to utilize the data from this investigation for any free stream velocity--propeller RPM combination, the non-dimensional parameter advance ratio (J) is used. Advance ratio is defined as:

$$J = \frac{V}{nD} \tag{10}$$

where V is the free stream velocity, n is propeller revolution in RPS and D is the propeller diameter in feet [Ref. 6:p. 28].

C. FLIGHT TEST

The flight test method utilized in this investigation makes the assumption that thrust and aircraft drag act through the same point and are parallel. For cruise performance in

steady flight conditions, the additional assumption is that the flight path angle is small such that [Ref. 5:p. 5.4]:

$$T = D \tag{11}$$

$$L = W \tag{12}$$

It is also assumed that due to the low flight test speeds involved, wave drag is negligible and the total drag can be written as follows:

$$C_D = C_{Do} + C_{Di} \tag{13}$$

Where C_D is the total drag coefficient, C_{Do} is the parasite drag coefficient and C_{Di} is the induced drag coefficient. C_{Di} can also be defined as:

$$C_{Di} = \frac{C_L^2}{\pi ARe} \tag{14}$$

Where C_L is the coefficient of lift, AR is the aspect ratio and e is the Oswald efficiency factor [Ref. 5:pp. 5.4-5.5]. The Oswald efficiency factor is an indication of how efficient the aircraft is. Combining Equations 13 and 14 gives the following equation:

$$C_D = C_{Do} + \frac{C_L^2}{\pi ARe} \tag{15}$$

The coefficients of lift and drag are defined as follows:

$$C_L = \frac{2L}{\rho_o V e^2 S} \tag{16}$$

$$C_D = \frac{2D}{\rho_o V e^2 S} \tag{17}$$

where ρ_o is sea level density, V_e is the equivalent velocity and S is the wing area [Ref. 5:p. 5.7].

From Equations 11 and 12, Equations 16 and 17 can be written:

$$C_L = \frac{2W}{\rho_o V e^2 S} \tag{18}$$

$$C_D = \frac{2T}{\rho_o V e^2 S} \tag{19}$$

where thrust (T) is determined from the following expression:

$$T = \frac{\eta SBHP_{ALT}}{V_T} \tag{20}$$

and the $SBHP_{ALT}$ can be found from:

$$SBHP_{ALT} = \sigma SBHP_{STD} \tag{21}$$

here σ is the test day density ratio [Ref. 9:p. 274]:

$$\sigma = \rho/\rho_o \tag{22}$$

The true velocity (V_T) was determined by timing the aircraft over a known distance over the ground. To compensate for wind effects two runs over the same course in opposite directions were performed while maintaining a constant magnetic heading. The true velocity was calculated by averaging the speeds for the two runs. The equivalent airspeed (V_e) is defined as [Ref. 9:p. 274]:

$$V_E = V_T \sigma^{1/2} \tag{23}$$

The relationship between C_L and C_D, as shown in Equation 15, is parabolic and a plot of C_L versus C_D is called the drag

polar. From the assumption of a parabolic drag polar, a plot of C_D versus C_L^2 is an equation of a straight line with C_{Do} being equal to the Y intercept and C_{Di} being equal to the slope [Ref. 5:p 5.5].

The power required plot also provides useful performance data. Since an aircraft can fly at many weights and altitudes, a data reduction scheme was used to reduce the flight test data to standard weight and altitude. The standardization technique used for this investigation was the P_{iw}-V_{iw} method. V_{iw} is defined as the true airspeed corrected to a standard weight and sea level conditions:

$$P_{iw} = \eta SBHP_{ALT} \left(\frac{W_s}{W_T} \right)^{3/2} (\sigma)^{1/2} \qquad (24)$$

where W_S is the standardized weight and W_T is the test weight. P_{iw} is defined as the power required corrected to standard weight, sea level conditions:

$$V_{iw} = V_T \left(\frac{W_s}{W_T} \right)^{1/2} (\sigma)^{1/2} \qquad (25)$$

Standard weight for this method is an arbitrary weight and for this investigation was chosen as the aircraft's gross weight. The final plot of P_{iw} versus V_{iw} provides useful performance data. The bottom of the curve indicates the minimum power required and therefore the velocity for maximum endurance. The tangent from the origin to the curve is the point of

maximum velocity per fuel or the velocity for maximum range. A plot of $P_{iw}V_{iw}$ versus V_{iw}^4 yields a straight line of the form:

$$P_{iw}V_{iw} = AV_{iw}^4 + B \tag{26}$$

where A is the slope of the line and B is the Y-intercept. From this information C_{Do} and e can be determined from [Ref. 5:pp. 5.11-5.13]:

$$C_{Do} = \frac{1100A}{\rho_o S} \tag{27}$$

$$e = \frac{W_s^2}{275\pi AR\ S\rho_o B} \tag{28}$$

Propeller RPM inflight was determined by recording the electrical signal generated by the RPM indication system discussed in Section IIIa, playing the tape back through a frequency counter and measuring the signal frequency (f). Propeller RPM was determined from the following calculation:

$$n = 30f \tag{29}$$

where n is propeller speed in RPM and f is the frequency in hertz.

The drag polar and power required curves can also be generated using the thrust generated from the wind tunnel tests rather than the power generated from the torque stand tests. In order to apply the wind tunnel thrust to inflight conditions the coefficient of thrust (C_T) must be defined:

$$C_{TE} = \frac{T_E}{\rho n^2 D^4} \tag{30}$$

where T_E is the effective thrust found in the wind tunnel runs, ρ is the wind tunnel air density, n is the propeller RPS and D is the propeller diameter [Ref. 5:p. 28]. If C_T is plotted versus advance ratio then C_T can be determined for any flight condition. For the advance ratios determined inflight, the C_T can be determined and the thrust (T) for that condition can also be calculated. Once this thrust is determined for all of the inflight test conditions, the C_D can be calculated using Equation 19. P_{iW} can be determined by solving for $\eta SBHP_{ALT}$ in Equation 20 and substituting into Equation 25 to get the following equation:

$$P_{iW} = \sigma T V_T \left(\frac{W_s}{W_T} \right)^{3/2} \sigma^{1/2} \qquad (31)$$

where T is the thrust determined from the plot of C_T versus J and from Equation 30 for each inflight test condition.

V. EXPERIMENTAL PROCEDURE

A. WIND TUNNEL TEST SECTION CALIBRATION

The wind tunnel test section calibration was conducted to determine the relationship between the actual free stream dynamic pressure (q) in the test section and the static pressure differential (Δp) across the contraction cone. This relationship was then used to determine the test section free stream velocity by measuring Δp.

In order to measure q in the test section a pitot-static tube was placed in the center of the test section. A hand held pressure transducer was connected across the total and static ports of the pitot-static probe to measure q. The static pressure differential across the contraction cone, Δp, was measured using the wind tunnel micro-manometer. The micro-manometer was connected across the two static port ring assemblies, one mounted in the plenum section and one mounted at the entrance to the test section. Delta P and q are linearly related and can be expressed as:

$$q = F\Delta p \tag{32}$$

where F is the Tunnel Calibration Factor. F is the slope of the line generated by plotting the measured values of q and Δp. Once F has been determined, test section q can be calculated using Equation 32 [Ref. 10:pp. A1-1-A1-6].

Calibration measurements were taken every 2 cm of water from 0 cm to 24 cm of water. Delta p and q were recorded for each calibration point and the data are listed in Appendix C, Table I. Figure 15 shows the plot of q versus Δp. The relationship was found to be linear and the tunnel calibration

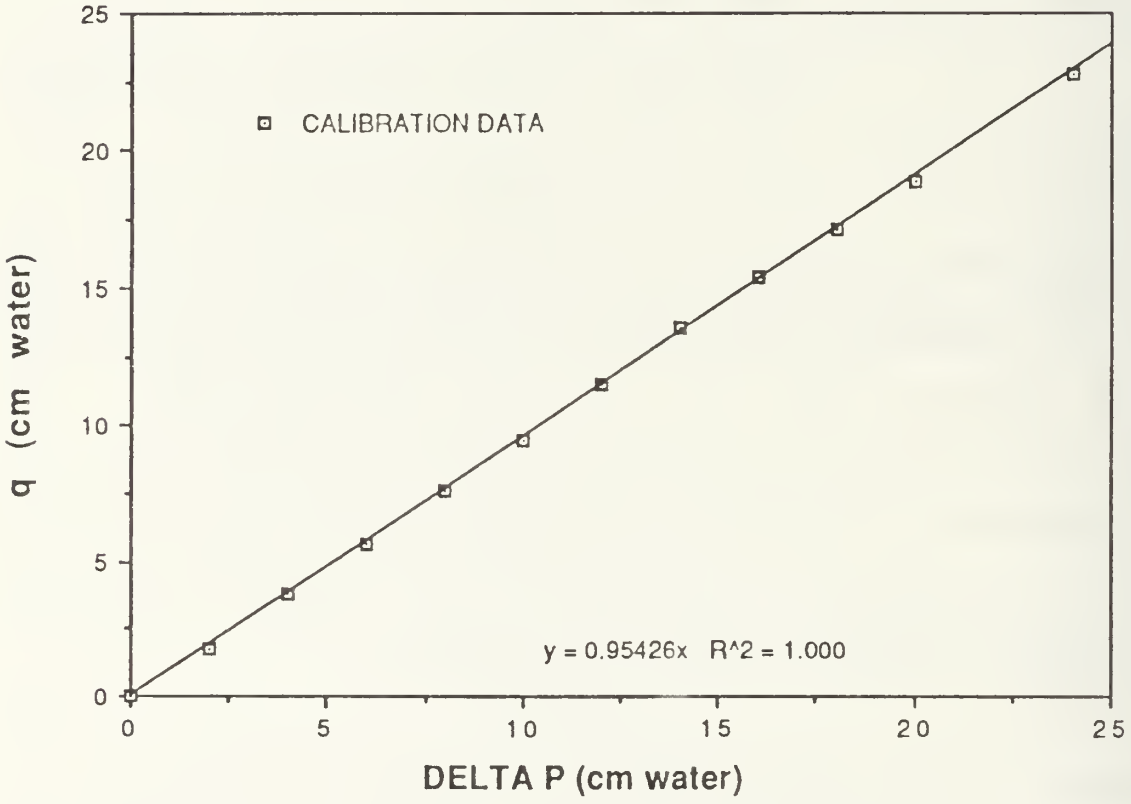

Figure 15. NPS Vertical Wind Tunnel Test Section Calibration

factor was determined to be 0.954. The wind tunnel test section free stream velocity was calculated from the following equation:

$$V = \left(\frac{2F\Delta P}{\rho} \right)^{1/2} \tag{33}$$

where Δp was measured from the micro-manometer board and converted to pounds per square foot and ρ is the density of the wind tunnel air in slugs per cubic foot determined from measurements of temperature and atmospheric pressure [Ref. 10:p. A1-4].

B. WIND TUNNEL BALANCE CALIBRATION

The wind tunnel balance was first checked to ensure that the strain gages were mounted properly. Each gage was checked individually using a Measurements Group P-3500 portable strain indicator. The balance was loaded statically with known weights and the resulting strain was recorded. The strain reading was then put into the proper equation relating strain and bending force generated shown in Appendix A. The bending force obtained from this equation was compared to the known static load. Each strain gage measured the bending force applied to the beam to within 5 percent of the actual reading. The 5 percent difference was attributed to stress concentrations caused by the "window" cutout. The balance was loaded and unloaded many times to ensure repeatability. The strain gage readings were repeatable to within 0.1

percent. Pairs of strain gages were also checked against each other. Since the window was symmetrical any stress concentration factors should affect each pair of strain gages equally. The values of strain obtained from gages one and four were within 1 percent of each other as were the values for gages two and three for each static load.

The balance was then calibrated with all four strain gages hooked up in the ten wire configuration to the Pacific Amplifier. The balance was statically loaded with a known weight. The excitation voltage on the amplifier was adjusted so that 0.0100 millivolts was equivalent to 1.00 pounds of force in the longitudinal direction along the thrust axis. The balance was then statically loaded for various known weights to ensure the readings were repeatable and that for the expected range of forces to be measured the balance readings were linear. The data obtained from this calibration are listed in Appendix C, Table II and the plot of the calibration force versus the DMM voltage output is shown in Figure 16. The plot shows a linear relationship between force and voltage output with a slope of 1.00.

Due to the orientation of the strain gages, the balance also measures the torque reaction of the electric motor. Because of this, during the wind tunnel tests, the DMM reading (R_{DMM}) gives a combination of the propeller thrust longitudinal force voltage reading (R) and the voltage reading due to

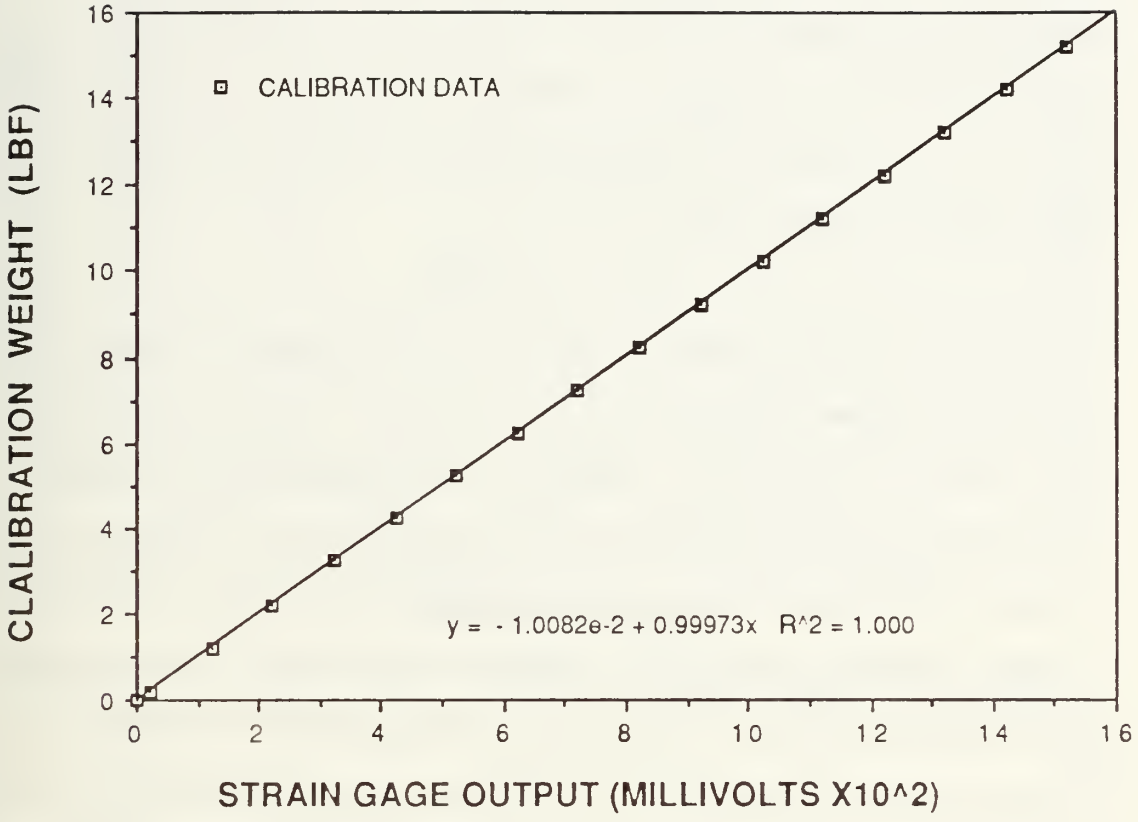

Figure 16. Wind Tunnel Balance Calibration Plot

engine torque (Q_{DMM}). In order to obtain the pure propeller thrust force (R) the following relationship was used:

$$R = R_{DMM} - Q_{DMM} \tag{34}$$

Q_{DMM} was determined by performing a calibration test in which the DMM output voltage was measured as the balance was loaded laterally with known weights. The data from this calibration are listed in Appendix C, Table III and a plot of output

voltage versus the applied torque was constructed as shown in Figure 17. The maximum torque generated by the test propeller was determined to be less than 1.00 ft-lbs and for this region the plot was linear and the slope was calculated as 0.175. The equation relating torque (Q) and output voltage (Q_{DMM}) was then developed as:

$$Q_{DMM} = 0.175\ Q \tag{35}$$

The force (F) generated by the 14 X 6 P test propeller was measured on the torque stand for various n's and these data are listed in Table IV, Appendix C. Equation 1 was used to calculate the engine torque (Q) from the force data for each n tested and these results are plotted as shown in Figure 18. A curve fit for these data were constructed using a least-square regression and the equation generated from this curve fit is shown on the plot. To correct the R_{DMM} reading to pure longitudinal force at each n tested in the wind tunnel, propeller torque (Q) for that RPM was calculated from the least-squares equation, Equation 35 determined the correction factor and substituting into Equation 34, the pure propeller horizontal thrust (R) was obtained. Q_{DMM} calibration data are listed in Appendix C, Table IV.

C. HALF-SCALE PIONEER RPM INDICATION SYSTEM CALIBRATION

The inflight engine RPM indication system was calibrated on the engine test stand. Figure 19 shows a close-up detail of the RPM indication system components for the half-scale

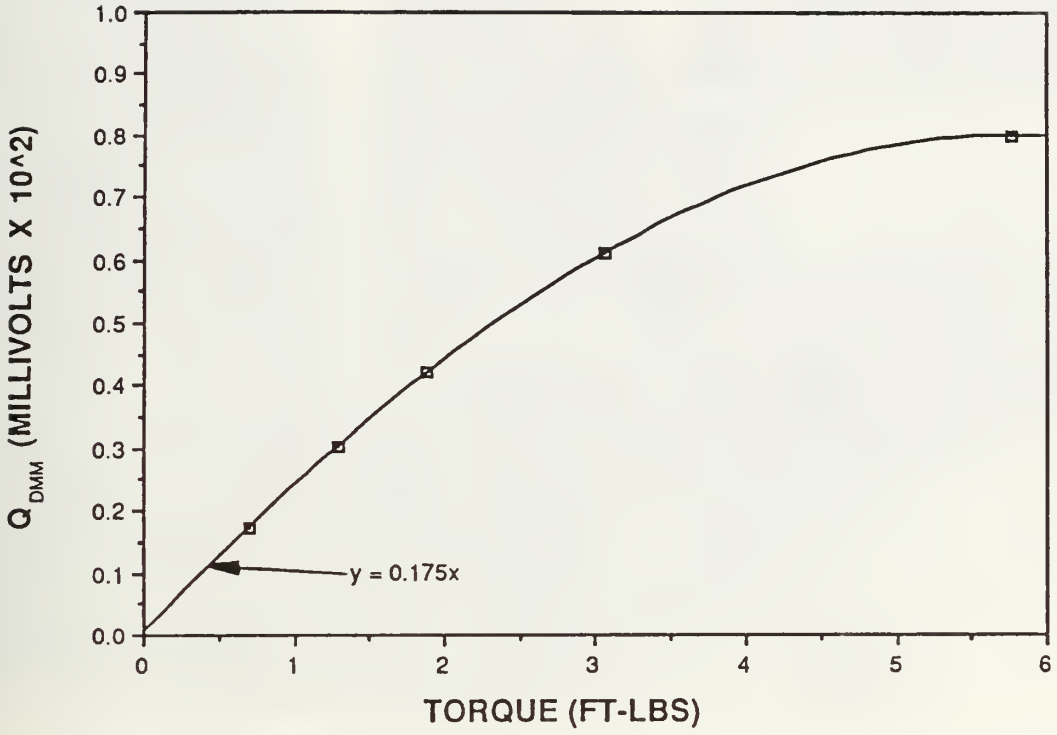

Figure 17. Wind Tunnel Balance Torque Correction Chart

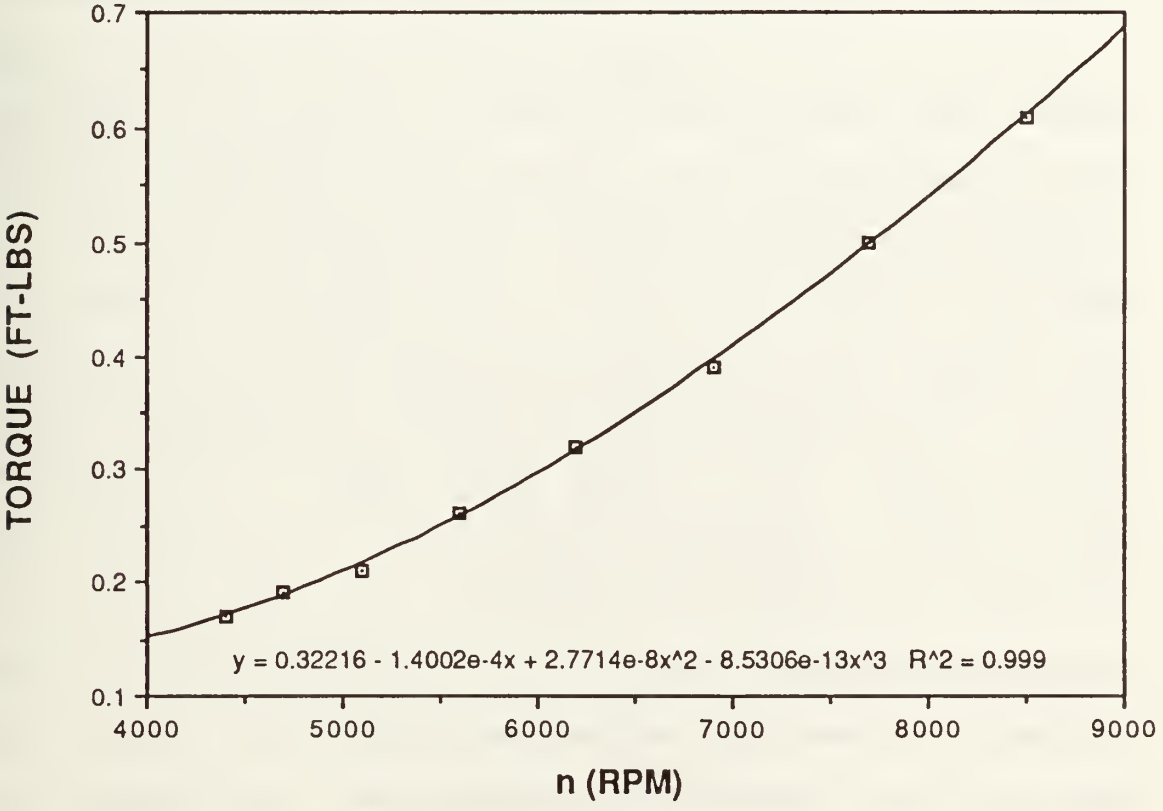

Figure 18. 14 X 6 Pusher Propeller Torque Plot

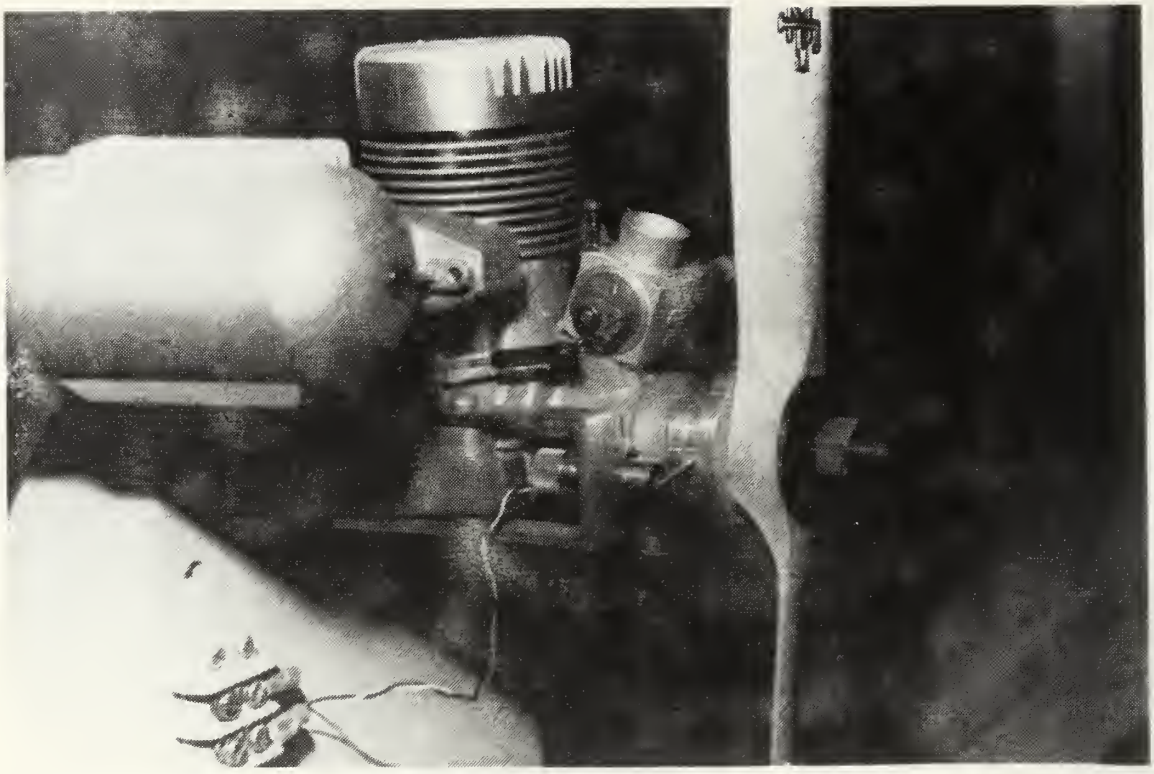

Figure 19. Engine Test Stand with RPM Indication System

engine. RPM for different throttle settings were measured with the magnetic proximity sensor/digital tachometer and with a optical tachometer attached to the Futaba transmitter and compared with the RPM obtained from recording the magnetic sensor signal and replaying the tape back through a frequency counter. This comparison showed that the inflight RPM system agreed with the optical method to ±100 RPM, or, for the range of inflight RPM, within 1.5 percent.

D. ENGINE BREAK-IN

The O.S. MAX-FSR engine was broken in as per the manufacturer's recommended instructions. The engine was

securely mounted to the engine test stand as shown in Figure 5. The break-in procedure consisted of running the engine at four-cycle operation for a period of three to four minutes and then two-cycle operation for approximately 30 seconds. This procedure was repeated, alternating between two-cycle and four-cycle operation while gradually increasing the four-cycle run time, until the fuel tank was empty. The fuel tank was refilled, the engine restarted and the needle valve was adjusted for maximum RPM. Once the engine maintained a steady speed the throttle adjustment on the carburetor was set to ensure steady idling and smooth acceleration at medium rotational speeds. To keep the engine from overheating during the break-in period only tractor propellers were used to ensure cooling airflow over the engine.

E. TORQUE STAND TESTS

Torque stand tests were conducted for the electric motor used in the wind tunnel test and for the half-scale Pioneer engine. The electric motor was mounted on the test stand as shown in Figure 20. The mount was designed so the center of rotation of the torque stand shaft and the electric motor shaft were aligned. The variable transformer voltage range was divided into equal settings and assigned a "percent throttle" setting with 140 volts corresponding to 100 percent throttle and 10 volts corresponding to 0 percent throttle. The assignment of these settings was arbitrary but necessary

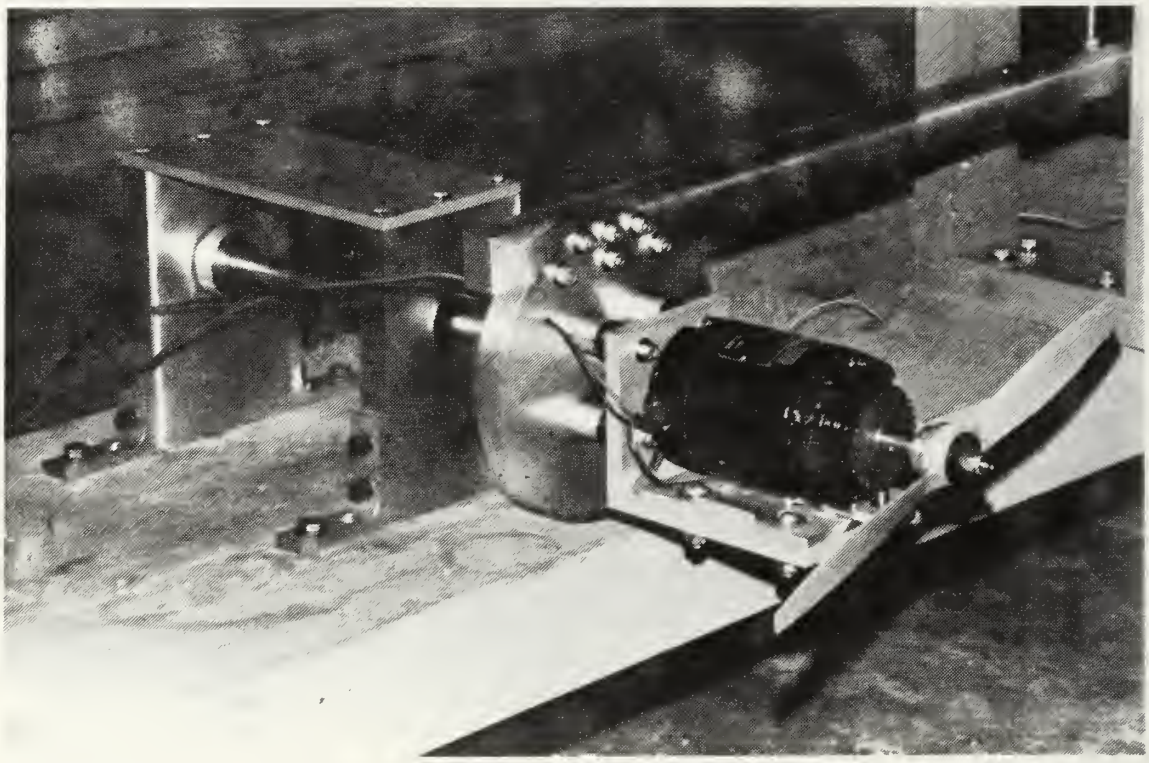

Figure 20. Electric Motor Mounted on Torque Stand

for purposes of repeated test conditions and the settings were used as reference points for all the tests which utilized the variable transformer and electric motor.

The electric motor $SBHP_T$ versus RPM was determined by loading the engine with different diameter propellers. Prior to the tests the propellers were reamed to the proper shaft size and then carefully balanced in order to minimize vibrations. To ensure adequate RPM coverage the following propellers were tested: 10 X 7, 11 X 8, 14 X 8, 16 X 8, 18 X 8, 20 X 8 and the 14 X 6 pusher test propeller.

The RPM and the associated force exerted on the scale by the torque arm were measured for throttle settings from 20 to

100 percent at 10 percent increments for each of the six propellers tested. Prior to each run and after each run a tare weight with the engine stopped was recorded and subtracted from the measured force. Force measurements for each of the wind tunnel RPM's were recorded with the test propeller installed so engine torque corrections (Q_{DMM}) could be applied to the wind tunnel test results as discussed in Section IVB.

The flight test vehicle engine was tested in the same manner as the electric motor. The engine was mounted on the torque stand as shown in Figure 21. The mount was designed so the torque stand shaft axis and the engine shaft axis were

Figure 21. Half-Scale Pioneer Engine Mounted on Torque Stand

aligned. The propellers used to vary the load for this test were a 12 X 9, 14 X 6 P, 14 X 8, 16 X 8 and a 18 X 8. The transmitter throttle position indicator was divided into 24 detent positions. This range of detents were divided equally into percent throttle readings with detent 24 equal to 100 percent throttle and detent 5 equal to 5 percent throttle. A change in one detent position corresponded to a 5 percent change in throttle. These settings were arbitrary and were used as reference positions for all tests done with this engine and transmitter. Propeller RPM and the associated force were recorded for each load and throttle setting. Prior to each run, the local barometric pressure, atmospheric temperature and partial pressure water vapor were recorded.

F. WIND TUNNEL TEST

Wind tunnel tests were conducted to determine the effective thrust required for the propulsive efficiency calculation. The wind tunnel model was mounted on the wind tunnel balance, as shown in Figures 11 and 12, at approximately the wing quarter chord point in order to minimize the bending contribution due to wing lift. The strain gage bridge resistance was measured to ensure proper hook-up. The amplifier was calibrated and the excitation voltage determined from the static calibration of 1.870 V was set. The propeller was removed from the model and the bridge was balanced. Prior to each run wind tunnel temperature and

pressure were recorded. The wind tunnel was turned on and the tunnel drive blade pitch was set for a test section ΔP of 2 cm of water as measured by the micro-manometer. Depending on tunnel temperature, pressure and calibration factor this corresponded to a test section speed of approximately 60 ft/s. The tunnel was allowed to stabilize and the system drag (D) was recorded from the DMM. The wind tunnel was shut down and the propeller was attached to the model motor drive shaft. The bridge was rebalanced, the wind tunnel was restarted and the tunnel drive blade pitch was set for a tunnel ΔP of 2 cm of water. The horizontal propeller thrust plus engine torque reading (R_{DMM}) was recorded from the DMM for predetermined values of RPM. To ensure the wind tunnel test and torque stand test were conducted for the same conditions, the voltage setting on the variable transformer for each RPM was noted. Motor voltage and RPM were the two values required to enter the $SBHP_{STD}$ versus RPM chart to obtain the power corresponding to the conditions of the wind tunnel. After each run the DMM output was checked to ensure a zero reading, and the tunnel temperature and pressure were recorded. The start and end tunnel temperatures were averaged and used to calculate wind tunnel velocity.

G. FLIGHT TEST

The day before each test flight the aircraft was readied for flight. The transmitter battery and aircraft battery pack

were recharged and the test instrumentation was installed and checked to ensure proper working order. The aircraft center of gravity was checked for full and empty fuel tanks for this configuration and weight was either added or subtracted from the dead weight in the nose to put the aircraft CG at 33 percent C_{MAC}. The method used to check aircraft center of gravity was to measure the weight on each wheel, sum moments around a fixed point on the aircraft and solve for the cg position.

Flight testing was conducted initially at Fritsche Army Airfield at Ft Ord, CA, and then switched to a grass strip near Los Banos, CA, due to intermittent radio interference from an unknown source at Fritsche Field. The aircraft was assembled and preflighted to ensure all components were securely fastened. Once the aircraft was preflighted and fueled, a transmitter-receiver check was accomplished to ensure proper working order and that there was no outside interference affecting the control signal. During this check the aircraft control surfaces were checked to ensure the transmitter neutral position corresponded to the control surface neutral position. The aircraft was started by energizing the engine glow plug with 1.5 volts from a ground starter control panel. This same control panel provided 12 volts to a hand held aircraft starter. Starting was accomplished by applying torque to the aircraft engine through a friction coupling between the starter and the propeller

spinner. The engine was allowed to warm-up and then tuned by ear for maximum performance by adjusting the engine needle valve.

The first flight of the day was conducted to warm-up both the engine and the pilot and to ensure the RPM indication system was working. During this flight the pilot also checked to see if the control surfaces for straight and level flight were approximately in the neutral position on the transmitter. After the initial flight the aircraft was refueled and the control surfaces were retrimmed as required. Prior to start the tape recorder and an elapsed time stop watch were started simultaneously. The engine was started and retuned for peak performance, and the aircraft was launched for the initial set of data runs.

The technique used to collect true velocity (V_T) data versus RPM for various throttle settings was the constant altitude method. Maximum throttle was set on the transmitter (detent 24) and aircraft speed was allowed to stabilize while maintaining a constant altitude. The true velocity was determined by timing the aircraft over a known distance marked on the ground. To compensate for any crosswind effects, two runs at the same throttle setting in opposite directions were performed while the aircraft was allowed to drift with crosswind. The elapsed time for each run was also noted so the RPM could be determined on the ground from the taped

signal. This process was completed for each throttle position.

VI. RESULTS

A. TORQUE STAND TESTS

The raw test data from the electric motor torque stand tests are listed in Table V, Appendix C. Equation 1 was used to determine engine torque (Q) for each load and throttle setting and Equation 2 was used to calculate the corresponding $SBHP_T$. Electric motor power data are listed in Table I, Appendix D and the $SBHP_T$ versus n plot for the electric motor is shown in Figure 22. A least-squares regression was used to curve fit data for each throttle setting. The parabolic shape of the curve for each throttle setting is typical for a piston engine-propeller combination. These curves were developed to provide SBHP information for any n and voltage tested in the wind tunnel. The number of propellers tested provided an adequate coverage over the range of test n's and helped in developing the overall curve shape.

The raw data from the half-scale Pioneer engine torque stand test are tabulated in Table VI, Appendix C. The method of determining $SBHP_T$ versus RPM was the same as that for the electric motor. Because the flight test engine was an air breathing engine, the $SBHP_T$ was corrected to standard day, sea level conditions using Equation 3. The half-scale Pioneer engine power data are listed in Table II, Appendix D. $SBHP_{STD}$

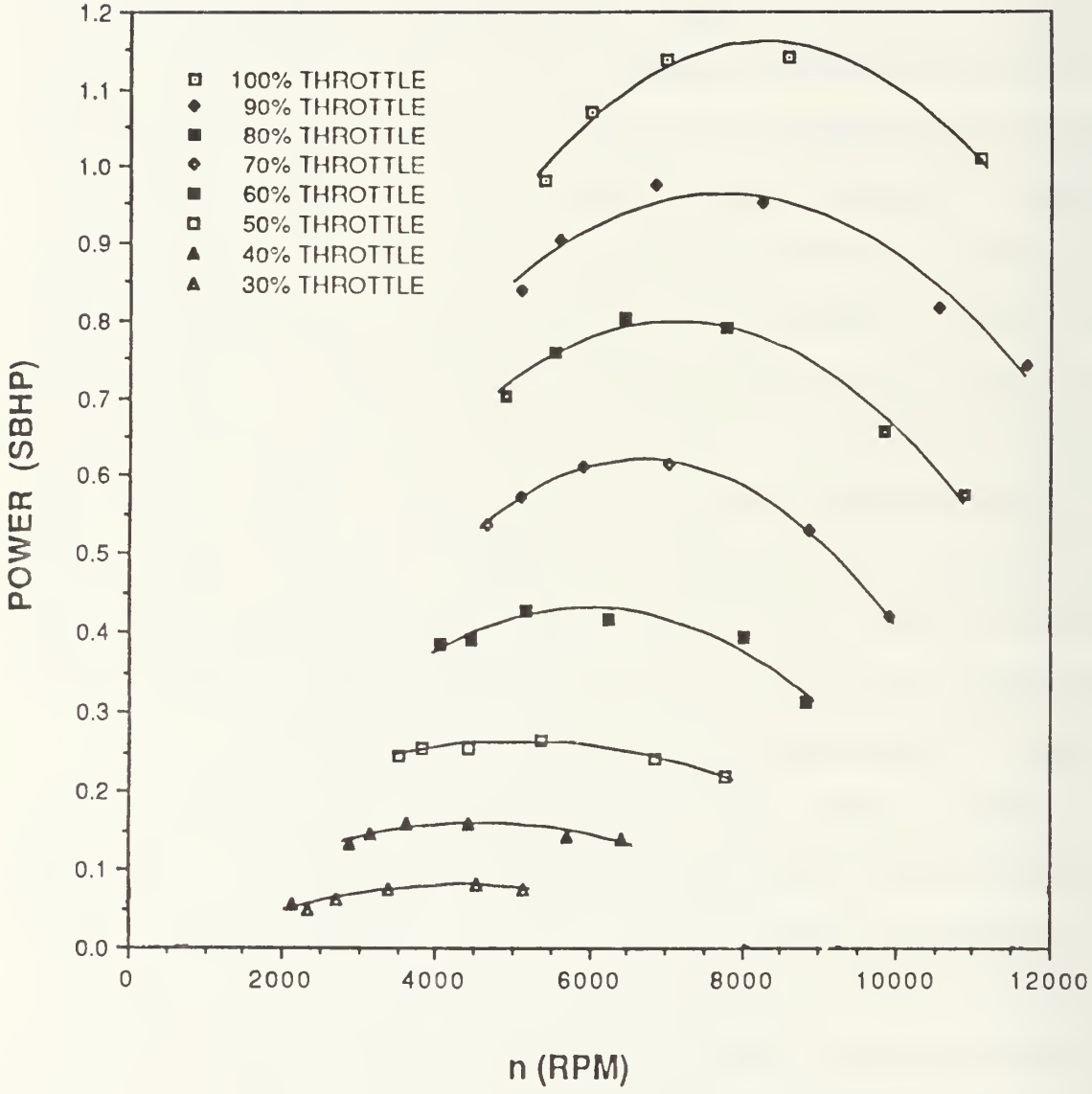

Figure 22. Electric Motor Power Curves

was determined for each throttle setting and load and is shown in Figure 23. The characteristic peak to these curves is not evident for all throttle settings, primarily due to the lack of testing a low load propeller. The advantages of testing a low load propeller for this case were determined insufficient compared to the disadvantage of overspeeding the engine or loosing a propeller. The cluster of curves for the higher throttle settings was due to the non-linearity of the engine throttle system. These curves were developed in order to determine inflight SBHP from the propeller rotational speed, which was easily measured inflight. The number of propellers tested to generate these curves was adequate to cover the range of n's encountered inflight.

B. WIND TUNNEL TEST

The raw data obtained from the wind tunnel tests are listed in Table VII, Appendix C. The propeller effective thrust was calculated by adding the horizontal propeller thrust (R), corrected for engine torque effects using Equation 33, and the system drag (D) for each n. The data used to determine the effective thrust and effective thrust coefficients for each n tested in the wind tunnel are listed in Table III, Appendix D. The effective thrust data were used to determine propeller efficiency. The plot of effective thrust (T_E) versus n is shown in Figure 24. The plot was generated in order to determine the behavior of the data

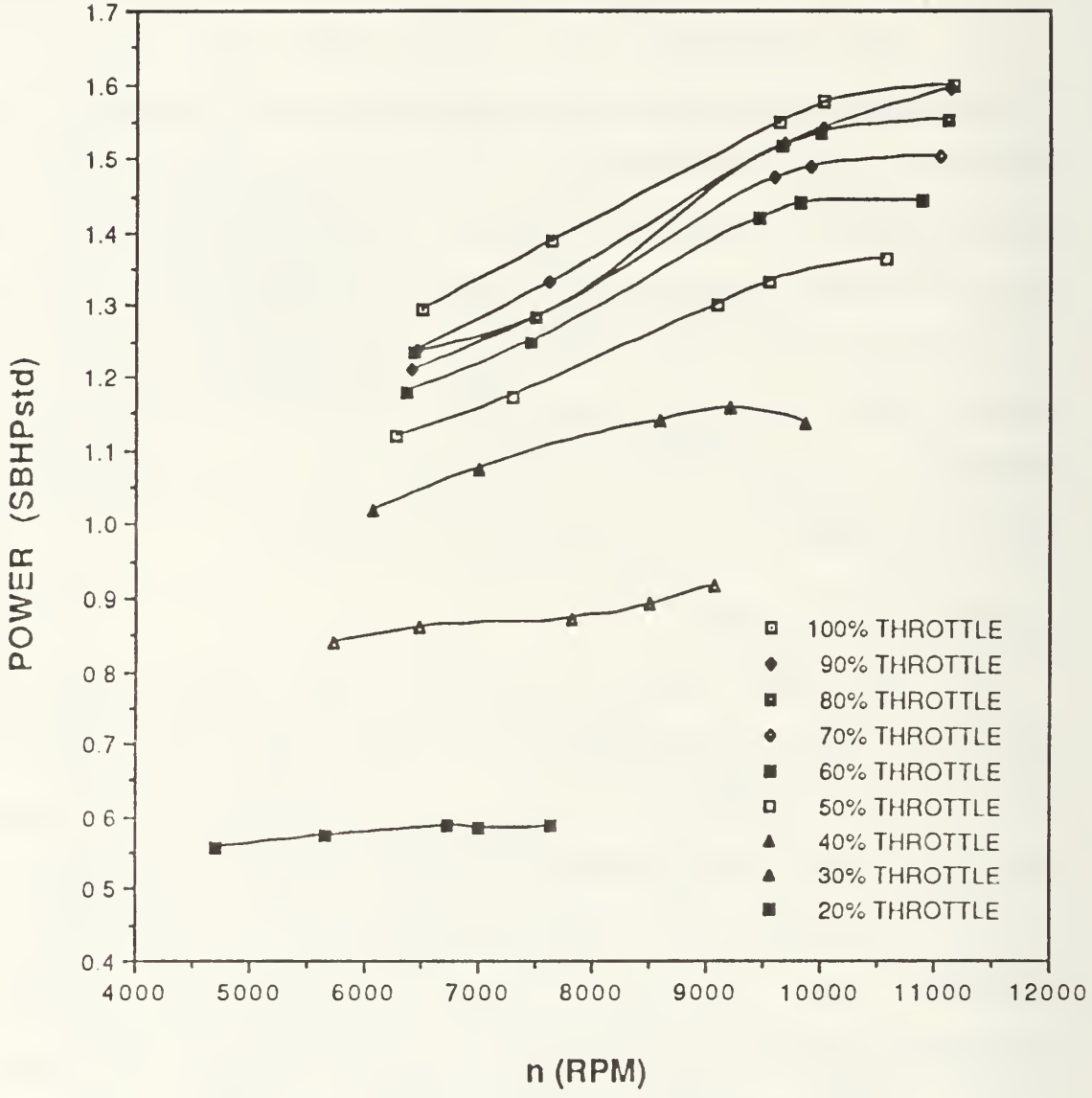

Figure 23. Half-Scale Pioneer Engineer Power Curves

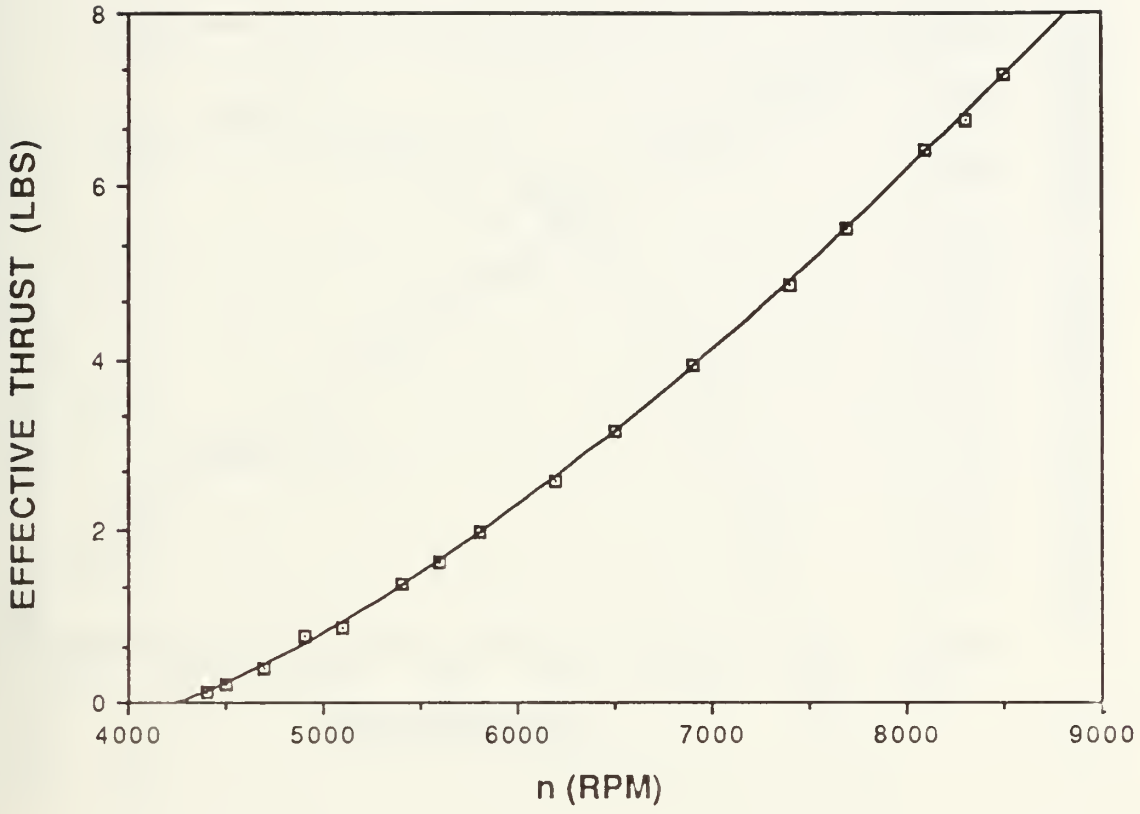

Figure 24. Effective Thrust Plot

generated from this test. The data plot behaves in an orderly fashion with little scatter. The effective thrust coefficient (C_{TE}) was determined using wind tunnel data and Equation 30 and plotted versus advance ratio as shown in Figure 25. This plot was then used to determine the effective thrust coefficient for the advance ratios determined during flight tests. These coefficients were used to calculate inflight thrust, again

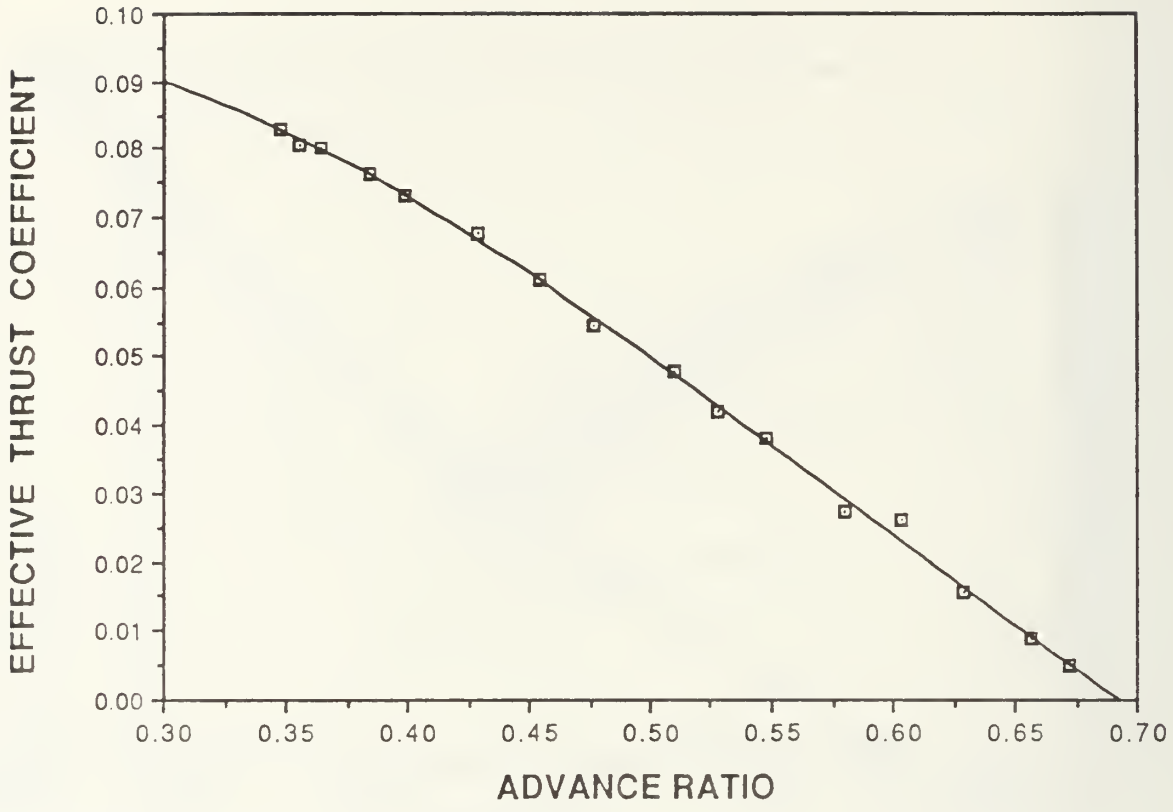

Figure 25. Effective Thrust Coefficient Plot

using Equation 30, and from this data drag polar and power required curves were generated.

Propeller efficiency for each n tested was calculated using Equation 9 and the data from the wind tunnel and torque stand tests and is listed in Table IV, Appendix D. The plot of propeller efficiency versus advance ratio is shown in Figure 26. The data are well behaved, show little scatter,

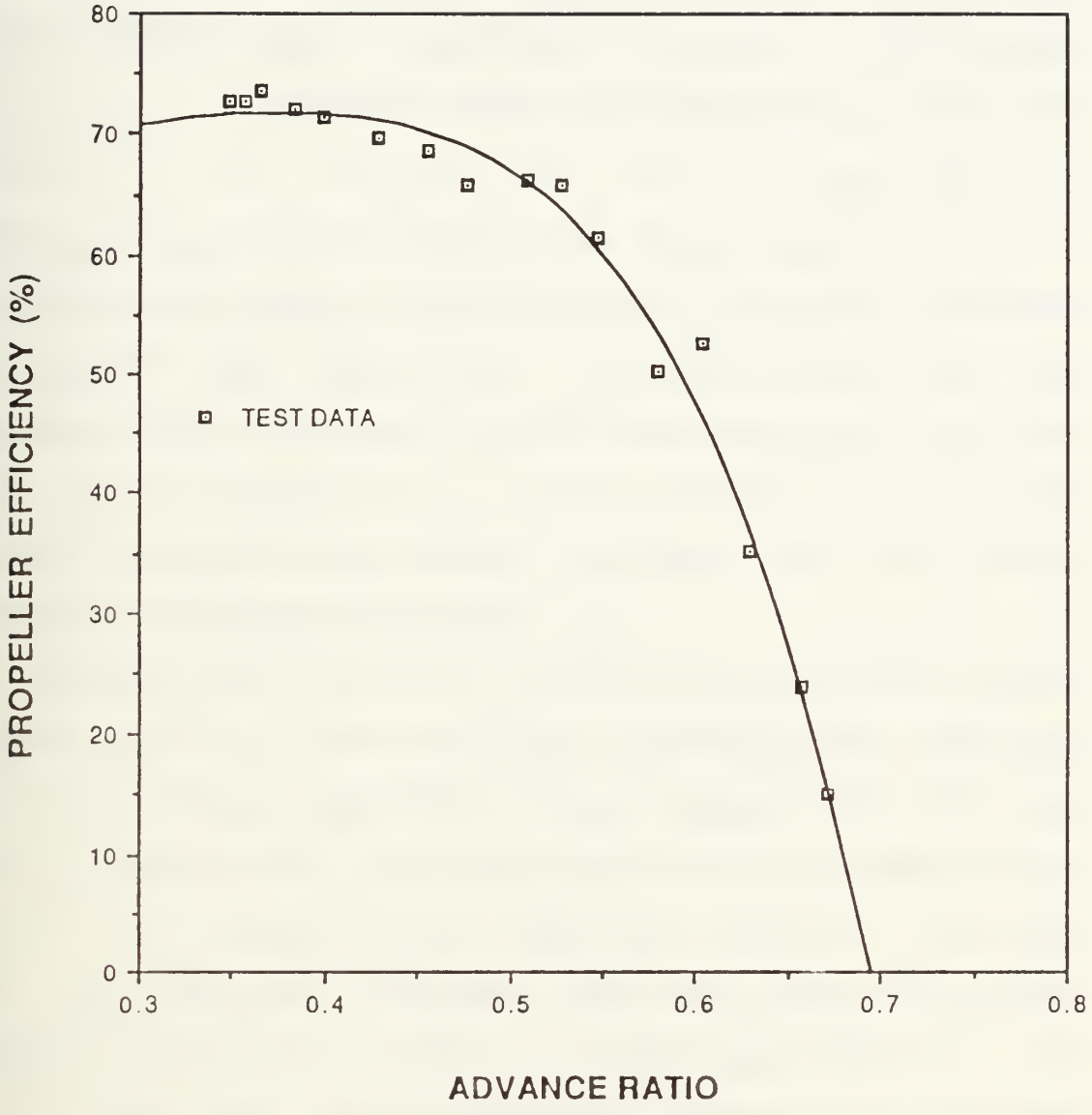

Figure 26. 14 X 6 Pusher Propeller Efficiency Chart

and exhibit the characteristic shape of the plots of this type. This plot was used to determine the propeller efficiency for the advance ratios measured during the flight test portion of this investigation so that inflight power required could be determined using Equation 4.

C. FLIGHT TEST

The aircraft true velocity (V_T) was determined by averaging the velocity calculated for each direction flown for each test throttle setting. The inflight tape of propeller frequency was played back through a frequency counter and the inflight RPM was determined for each throttle setting using Equation 29. The flight test raw data are tabulated in Table VIII, Appendix C. For each throttle setting the inflight advance ratio was calculated and Figure 26 was used to determine the associated propeller efficiency. The $SBHP_{STD}$ found from the engine torque stand tests was corrected to flight test conditions using Equation 21. The inflight power required was then calculated using Equation 22. This procedure was done for each throttle setting tested. The power required versus velocity data were then standardized using the P_{iw}-V_{iw} method. The standard weight (W_s) used in this analysis was 27.0 lbs and the test weight (W_T) was determined from fuel flow data and the elapsed time for each throttle setting. Power and velocity were corrected to standard weight, standard day conditions using Equations 24 and 25.

The smooth flight test data are listed in Table V, Appendix D and the power required data are listed in Table VI, Appendix D. The P_{iw} versus V_{iw} plot is shown in Figure 27. The solid line curve fit through these data points was carried out by plotting the equation of the line generated from the $P_{iw}V_{iw}$ versus V_{iw}^4 linear regression plot shown in Figure 28. This method is a standard flight test data analysis reduction technique. The Oswald efficiency factor, e, and C_{Do} for this method were determined using Equations 27 and 28 and the constants generated from the linear regression and were 0.0513 and 0.226 respectively. The P_{iw} versus V_{iw} plot also determined a velocity for maximum endurance of 55 ft/s and a maximum endurance velocity of 74 ft/s.

The half-scale Pioneer drag polar is shown in Figure 29. The data points for this plot were determined using Equations 19 and 20 and the applicable data developed from the wind tunnel, torque stand and flight tests (Table V, Appendix D) and are listed in Table VII, Appendix D. The solid line curve fit came from the equation generated from the linear regression plot of C_D versus C_L^2 as shown in Figure 30. The cluster of points on this plot was due to the non-linearity effects of the throttle position discussed earlier in this section. From the slope and Y-intercept of the linear regression equation, the C_{Do} and e for this method were determined to be 0.0516 and 0.221 respectively.

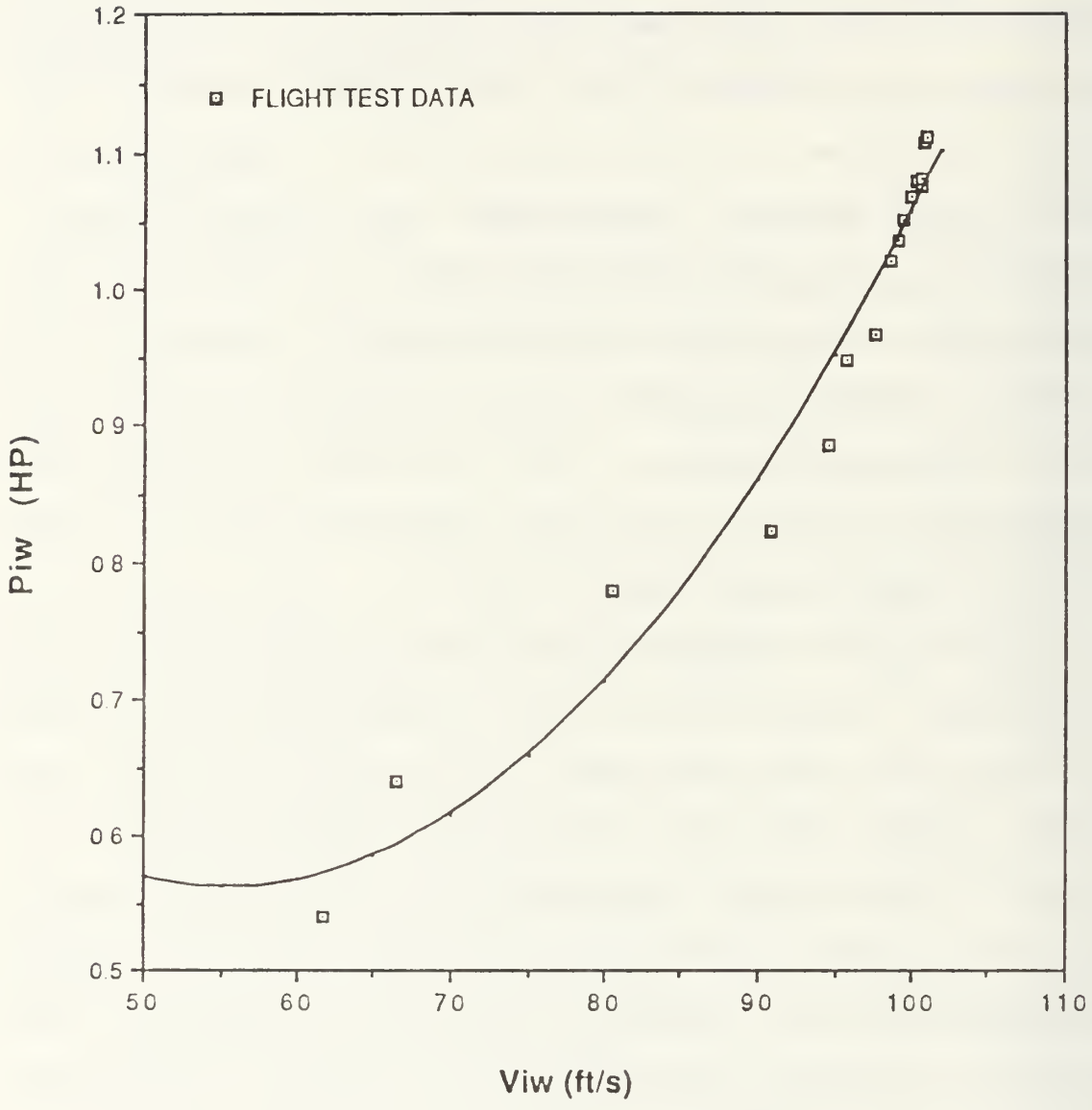

Figure 27. Half-Scale Pioneer Power Required Curve

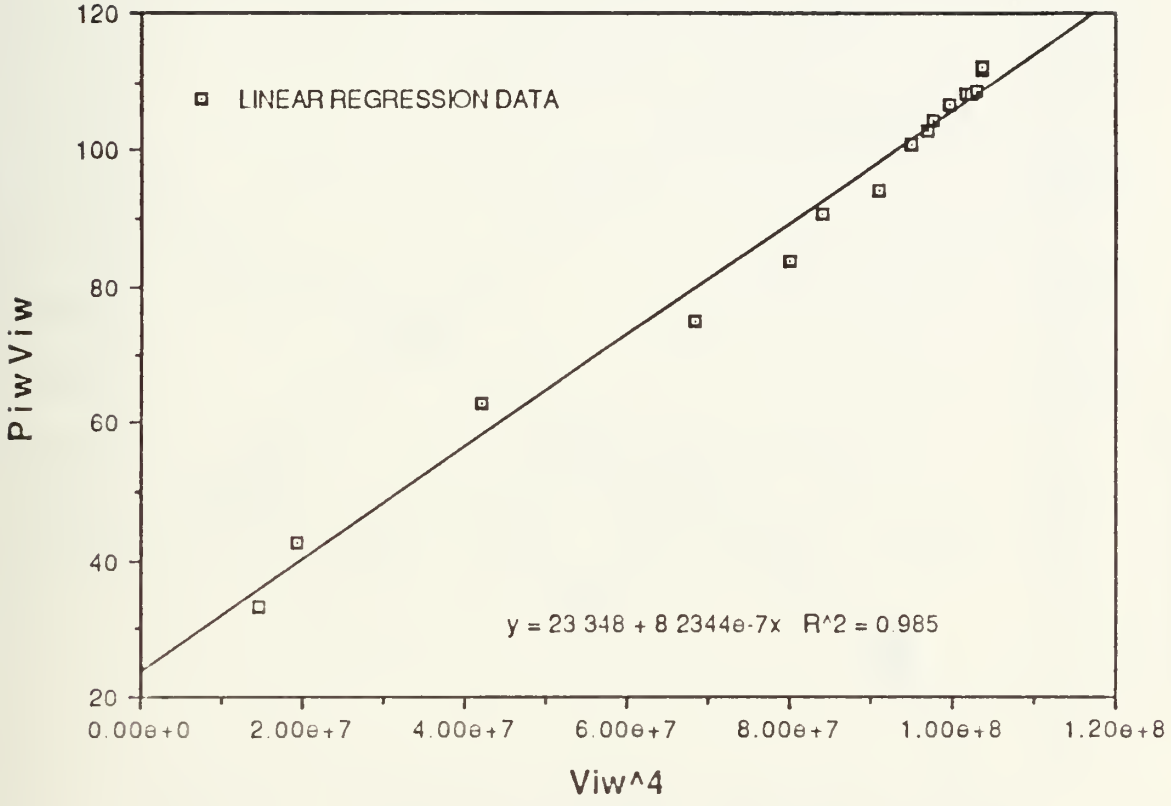

Figure 28. Power Required Linear Regression Plot

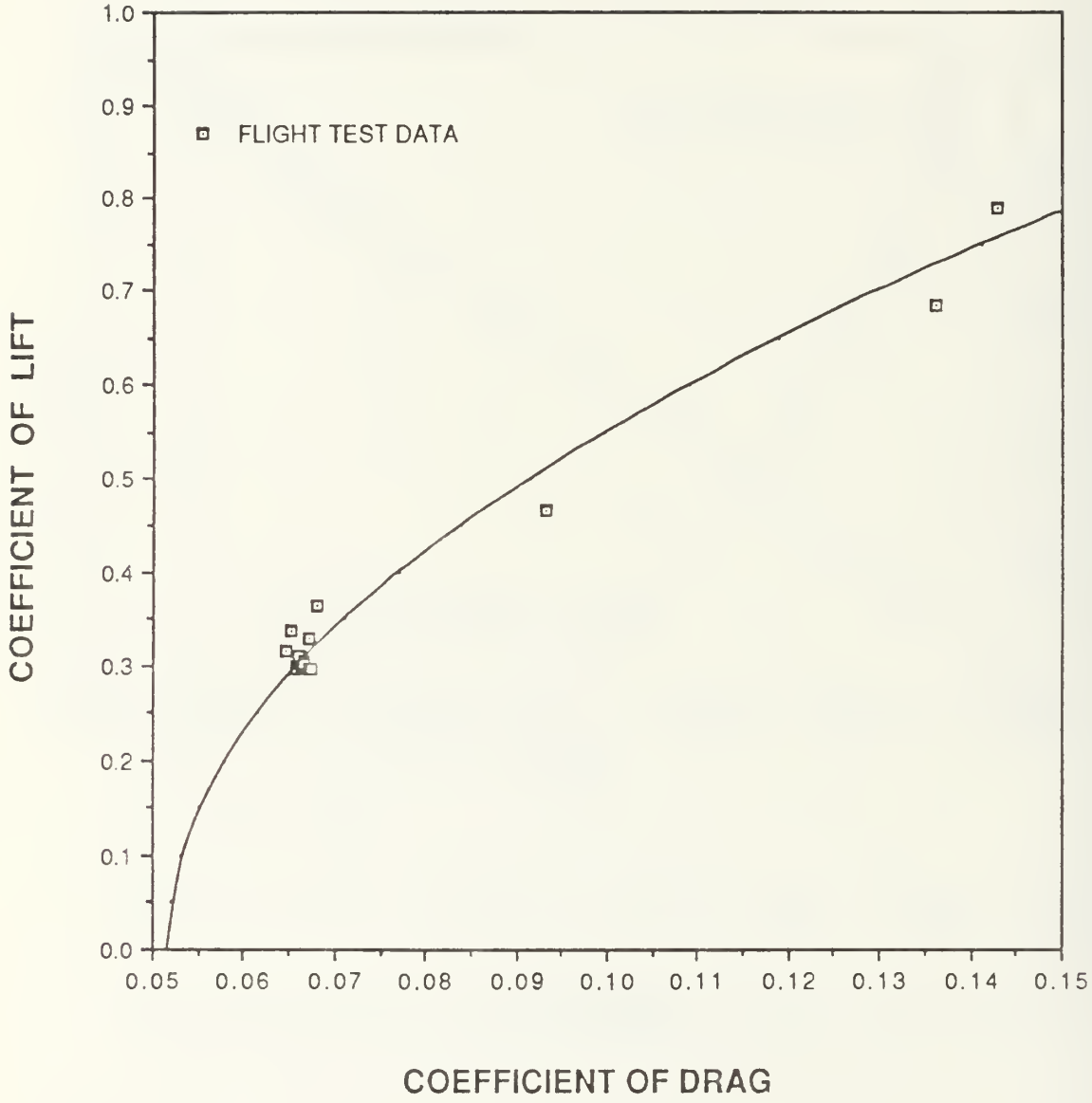

Figure 29. Half-Scale Pioneer Drag Polar Curve

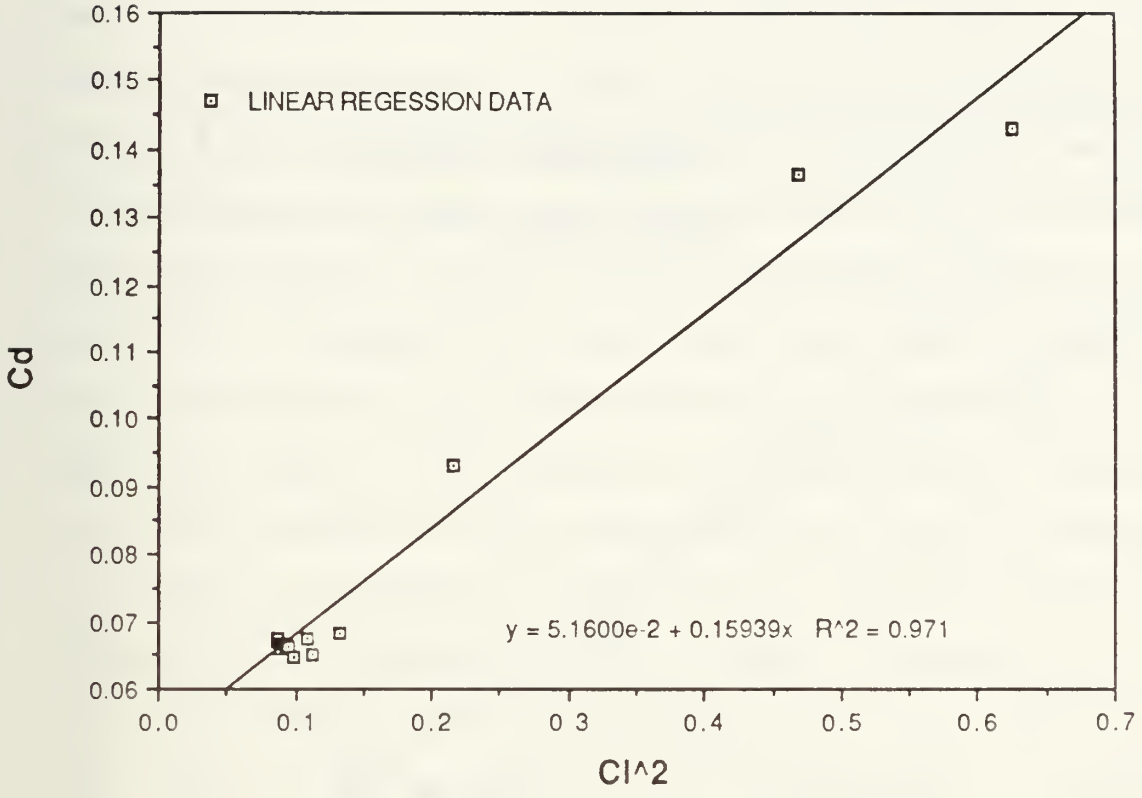

Figure 30. Drag Polar Linear Regression Plot

Another method of obtaining the power required and drag polar curves uses the propeller thrust determined from the wind tunnel test. From the C_{TE} versus advance ratio plot (Figure 25) the inflight thrust was determined using Equation 30 for the inflight n and advance ratio data. Substituting these thrust values into Equation 19 to find C_D and plotting these data versus C_L, the aircraft drag polar values using the

wind tunnel thrust data were generated and are listed in Table VIII, Appendix D. This plot was analyzed in the same manner as the drag polar obtained using the power generated from the torque stand tests. The two drag polars are plotted together in Figure 31 for comparison purposes. The C_{D_o} and e obtained from this method were 0.0697 and 0.371 respectively.

The thrust method can also be applied to generating power required curves. Using the thrust and Equation 31, P_{i_w} data can be generated and plotted versus V_{i_w}. The data for this plot are listed in Table IX, Appendix D. These data were analyzed as for the power method and are plotted with the power method power required data for comparison purposes as shown in Figure 32. The C_{D_o} and e obtained from this method were 0.0621 and 0.197 respectively. The maximum endurance velocity was determined to be 55 ft/s and the maximum range velocity was 70 ft/s.

The performance characteristics obtained from the drag polar agree closely with the characteristics obtained from the power required curves for each method. For all methods the Oswald efficiency factor was low. This was an indication that the high aspect ratio wing on the high drag body was not the most efficient combination.

The two methods used to obtain the drag polar and power required curves, as shown in Figures 31 and 32, differ significantly in the performance values obtained. The power required and drag polar curve developed using the data

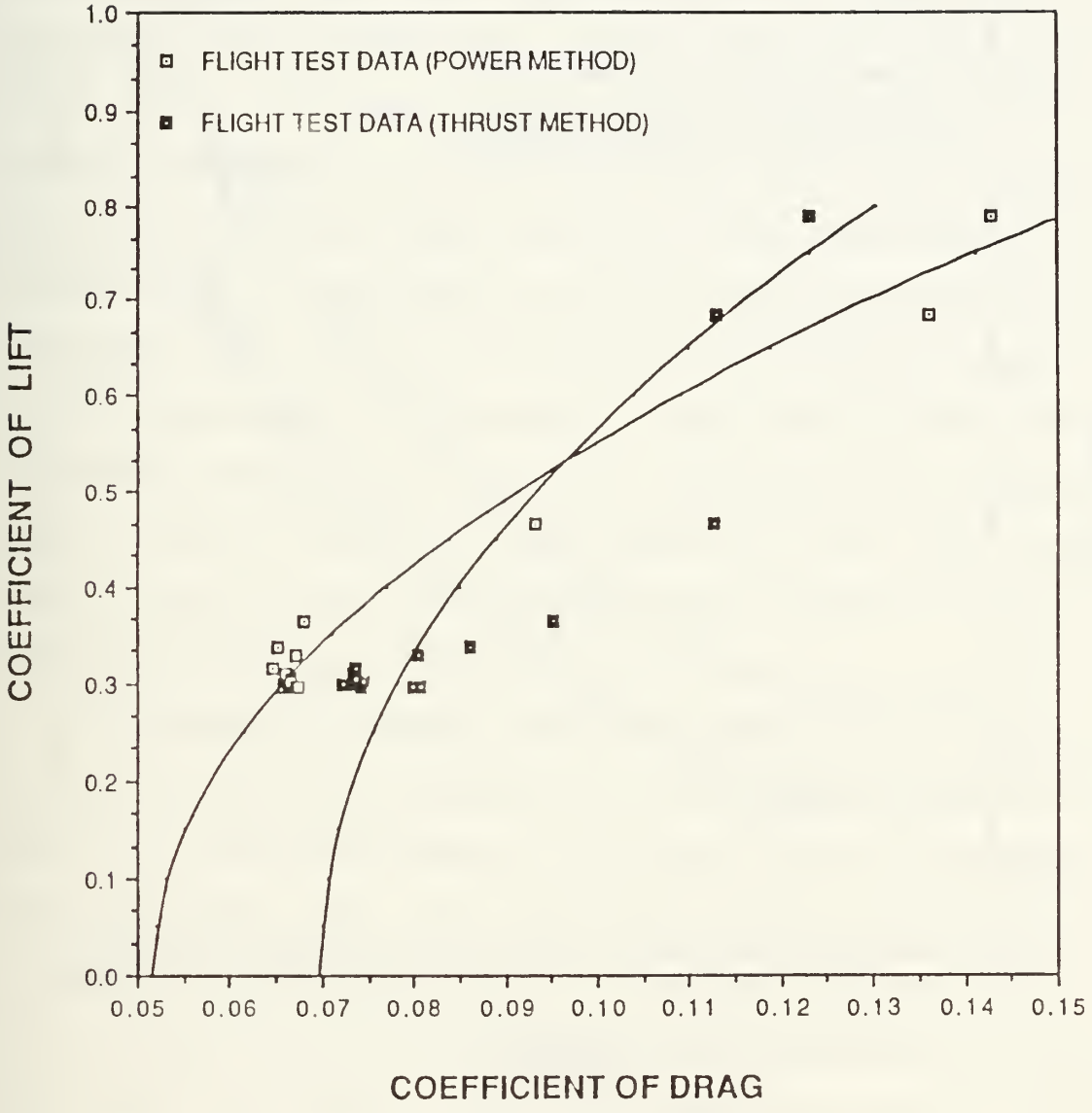

Figure 31. Half-Scale Pioneer Drag Polar Comparison Plot

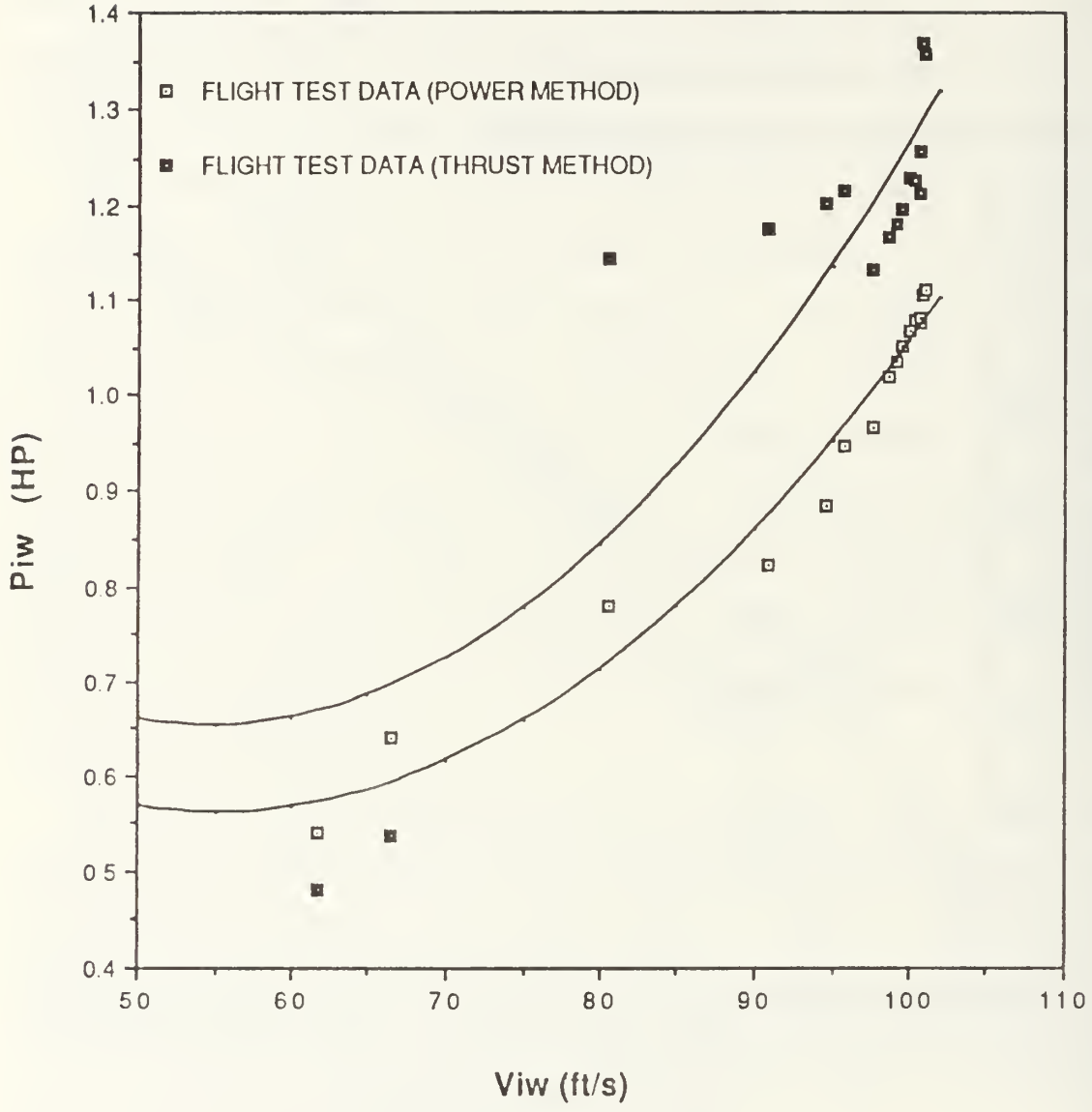

Figure 32. Half-Scale Pioneer Drag Power Required Comparison Plot

determined from the torque stand predicts higher drag for the same lift and less power required for the same velocity than the curves developed from wind tunnel thrust data. One possible reason for this difference is in the type of propellers used in each test. For the tests conducted on the torque stand, the power curves were constructed using only tractor propellers. In the wind tunnel test, only the test pusher propeller was used. The air flow generated by the tractor propeller provided cooling air over the motor during the torque stand tests. The combination of a pusher propeller and the position of the motor in the wind tunnel model resulted in little cooling air flow. This may have caused the electric motor to work more efficiently on the torque stand than it did for the wind tunnel tests resulting in the differences noted in these curves.

The scatter in the data for the thrust method may lie in the accuracy of the measurement of the propeller rotational speed, n. The thrust method, in the use of the C_{TE} equation, uses the square of n, and from the RPM indication system calibration, inflight measurement of n has, at best, a ±100 RPM accuracy. In order to determine the significance of this uncertainty in n, the C_D was calculated for n plus 100 RPM and n minus 100 RPM for each method. The error in C_D determined from the power data generated from the torque stand data was 1.8 percent and the error in the C_D determined from the thrust data generated from wind tunnel data was 10.7

percent. The ±100 RPM accuracy in n results in a factor of five difference in the C_D calculation between the two methods with the power method being the most accurate method.

VII. CONCLUSIONS AND RECOMMENDATIONS

A. CONCLUSIONS

The goal of this investigation was to develop a methodology to predict basic aircraft performance. This methodology consisted of wind tunnel and torque stand tests to determine propeller efficiency, torque stand tests to determine powerplant characteristics and flight tests to determine inflight propeller RPM for various flight speeds. The data from these three phases were then used to determine the power required and drag polar curves for the half-scale Pioneer.

This investigation was able to determine the basic performance characteristics and the results obtained appear reasonable for the aircraft tested within the constraints of the instrumentation. The method of obtaining propeller efficiency and static SBHP worked well and is the best alternative until inflight measurement of propeller thrust is developed. The flight test methodology and analysis of the data also worked well in the development of the required curves.

Since the purpose of this paper was not to obtain the half-scale Pioneer performance characteristics, the next logical step for the UAV program is to begin generating a data base so a more indepth analysis can be completed, and the

basic performance characteristics calculated in this investigation can be validated. Future plans for the half-scale Pioneer include the installation of a rate sensor package, autopilot system and a down-link telemetry system. The rate sensor package will allow a quantitative determination of the flying qualitues of the vehicle. The down-link will provide real time inflight test data.

Once the performance and stability characteristics are determined and validated through further testing, the vehicle will be ready to be used as a research tool for test, evaluation and validation of design changes to these type vehicles and as a test bed vehicle for other research projects. The UAV program has the capacity of providing another dimension to the Department of Aeronautics and Astronautics research capability.

B. RECOMMENDATIONS

There are several recommendations to be made for future research into UAV flight testing. These recommendations are broken down into the three phases of experimentation and include: wind tunnel testing, torque stand tests and flight tests.

1. Wind Tunnel Tests

The use of an electric motor as the wind tunnel model powerplant worked well and eliminated the problems associated in working with an air breathing engine. However, the effects

of electric motor heating on the motor efficiency, need to be investigated. One method to minimize the heating effects would be to measure engine torque and propeller thrust at the same time in the wind tunnel. This could be accomplished by adding four more strain gages to the wind tunnel balance oriented to measure the bending moment due to the motor torque.

To improve the wind tunnel data, the voltage to the wind tunnel model powerplant should be regulated and a more accurate way of measuring that voltage should be investigated. This would provide a steady power source to the motor which would improve the RPM measurement accuracy.

Efforts are being made at this time to improve the NPS vertical wind tunnel. Honeycomb and fine mesh screens are being installed in the plenum section which should reduce the swirl and lower the wind tunnel turbulence level. Also a data acquisition system is being installed which should increase the accuracy of the measurement of wind tunnel velocity and propeller thrust data. Once the screens and data acquisition system are installed, the wind tunnel tests conducted in this investigation should be completed again, and the results compared.

2. Torque Stand Tests

The plywood shielding installed to eliminate the prop wash from impinging on the torque arm and scale needs to be redesigned. The shield was positioned approximately 14 inches behind the propeller disk plane, and it may have affected the

flow of air through the disk plane. The torque arm and scale need to be protected in a less intrusive manner.

The mechanical scale used to measure the engine torque was adequate for this investigation. A digital load cell was first utilized but did not work well due to engine vibration. The large mass inertia effects of the scale provided natural damping which minimized these vibrations. However, as can be seen from Figure 21, the scale platform was 3 to 4 inches higher than the horizontal position of the torque arm. Although a geometric correction was applied to account for this, a scale which would allow measurements to be made with the torque arm horizontal would provide better accuracy.

3. Flight Test

The RPM signal measured inflight was noisy and had to be amplified and filtered prior to analysis with a frequency counter. Onboard signal amplification and filtering prior to taping would improve and standardize the taped signal for analysis by the frequency counter, and thereby increase the accuracy of the inflight propeller measurement.

The inflight method of determining the power available curves for the half-scale Pioneer needs to be investigated. This could be accomplished by installing an altimeter, measuring the vehicles excess power through rate of climb tests and adding this excess power to the appropriate power required curves.

APPENDIX A

HALF-SCALE PIONEER SPECIFICATION SUMMARY

TOTAL LENGTH:	5.92 FT
FUSELAGE LENGTH:	4.17 FT
WING SPAN:	8.19 FT
WING CHORD:	0.91 FT
WING ASPECT RATIO:	9.03
GROSS WEIGHT:	27.00 LBS
WING LOADING:	3.64 LBS/FT^2
CG LOCATION:	33% C_{MAC}
HORIZONTAL TAIL SPAN:	1.53 FT
HORIZONTAL TAIL CHORD:	0.50 FT
HORIZONTAL TAIL AREA:	0.77 FT^2
HORIZONTAL TAIL ASPECT RATIO:	3.06
HORIZONTAL TAIL VOLUME:	2.34 FT^3
VERTICAL TAIL SPAN:	1.01 FT
VERTICAL TAIL CHORD:	0.50 FT
VERTICAL TAIL AREA (2):	1.01 FT^2
VERTICAL TAIL ASPECT RATIO(1):	2.02
VERTICAL TAIL VOLUME (2):	3.09 FT^3

APPENDIX B

WIND TUNNEL BALANCE/STRAIN GAGE THEORY

A horizontal force acting on a rectangular beam, as shown in Figure B.1, can be found by measuring the bending moment, M_B, at a known distance, l, using the following relationship:

$$F = \frac{M_B}{l} \qquad (B.1)$$

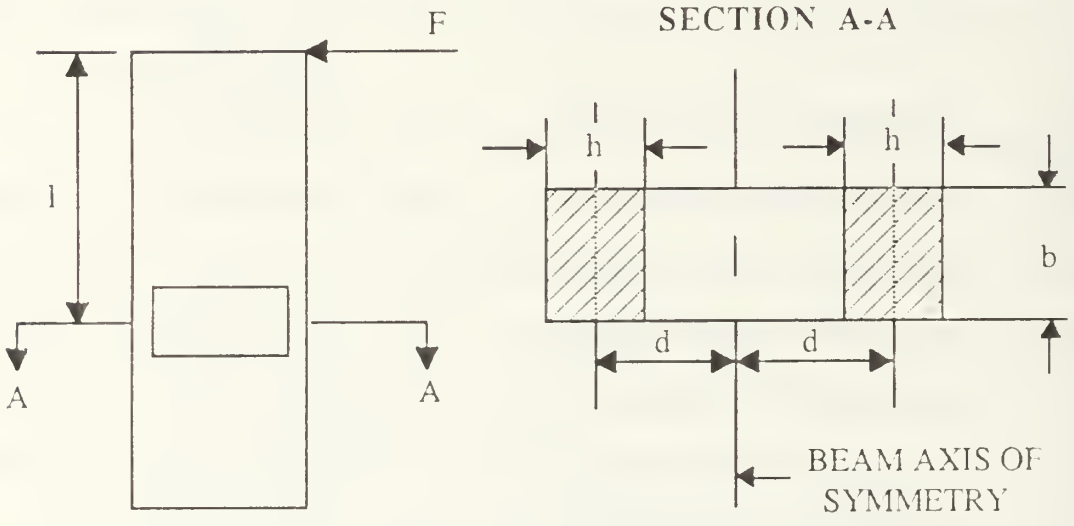

Figure B.1. Wind Tunnel Balance Theory Detail Diagram

The bending moment, M_B, is a function of the bending stress, σ_B, and can be determined for any distance c from the beam neutral axis from the following [Ref. 11:p. 157]:

$$M_B = \frac{\sigma_B I}{C} \tag{B.2}$$

The "window" cutout described in Section IIID reduces the beam cross-sectional area and changes the main beam into two smaller beam elements as shown in the section A-A detail in Figure B.1. Since both beam elements have the same dimensions and are symmetric about the beam axis of symmetry, the moment of inertia of the beam elements can be written as:

$$I = 2\left[\frac{bh^3}{12} + Ad^2\right] \tag{B.3}$$

where b is the beam width, h is the depth of each beam element, A is the cross-sectional area of each beam element and d is the distance between the beam axis of symmetry and each beam element axis of symmetry [Ref. 11:p. 582].

The beam bending stress for small deformations is directly proportional to the beam strain and is related as follows:

$$\sigma_B = E\epsilon_B \tag{B.4}$$

where ϵ_B is the beam strain due to the horizontal force and E is the material modulus of elasticity [Ref. 11:p. 156]. Combining Equations B.1, B.2, B.3 and B.4, the equation for the horizontal force can be written:

$$F = \frac{2E\epsilon_B}{Cl}\left[\frac{bh^3}{12} + bh^2d\right] \tag{B.5}$$

For this investigation the beam width, b, was 0.500 inches, the individual beam depth, h, was 0.375 inches, the moment arm, l, was 14.906 inches and d was 1.313 inches. The value of c for strain gages one and four was 1.500 inches and for strain gages two and three was 1.125 inches.

The beam strain was measured using four bonded, electrical-resistance type strain gages mounted as shown in Figures 8 and 10. Strain gages of this type are based on the principle that electrical resistance of the strain gage wiring changes when subjected to a mechanical deformation. The strain gages were bonded to the aluminum beam under no load conditions. When the horizontal force was applied, the beam and the strain gages were subjected to a deformation. The deformation caused a change in gage resistance which was measured as a change in voltage on the DMM. The balance calibration described in Section VB determined the relationship used in the wind tunnel test between the horizontal force and the DMM voltage output.

Equation B.5 was used to ensure each gage was bonded to the balance beam correctly. The balance was loaded statically with a known weight and for each weight the beam strain was measured using a strain measurement indicator. Equation B.5 was then utilized to determine the force required to produce this strain. If the force determined from Equation B.5 and the known load where equal, then the gages were assumed to be bonded to the beam correctly.

APPENDIX C

RAW DATA TABLES

TABLE I

VERTICAL WIND TUNNEL CALIBRATION DATA

ΔP (CM WATER)	q (CM WATER)
0.00	0.00
2.00	1.75
4.00	3.80
6.00	5.65
8.00	7.55
10.00	9.40
12.00	11.50
14.00	13.50
16.00	15.40
18.00	17.10
20.00	18.90

DATE: 12-16-88
TEMPERATURE: 67.0 F
PRESSURE: 30.09 IN HG

TABLE II

WIND TUNNEL BALANCE CALIBRATION DATA
(LONGITUDINAL DIRECTION)

STRAIN GAGE OUTPUT (MILLIVOLTS D.C.)	WEIGHT ON BALANCE (LBF)
0.0000	0.00
0.0022	0.21
0.0122	1.21
0.0223	2.21
0.0322	3.21
0.0424	4.21
0.0522	5.21
0.0621	6.21
0.0720	7.21
0.0820	8.21
0.0922	9.21
0.1024	10.21
0.1123	11.21
0.1224	12.21
0.1322	13.21
0.1421	14.21
0.1522	15.21

EXCITATION VOLTAGE = 1.870 VOLTS

DATE: 1-22-89

TABLE III

WIND TUNNEL BALANCE CALIBRATION
(LATERAL DIRECTION)

STRAIN GAGE OUTPUT (MILLIVOLTS D.C.)	BALANCE LOAD (LBF)
0.00000	0.00
0.00175	1.21
0.00305	2.21
0.00420	3.21
0.00610	5.21
0.00800	7.21

EXCITATION VOLTAGE = 1.870 VOLTS

DATE: 01-20-89

TABLE IV

TORQUE STAND CALIBRATION DATA
FOR 14 X 6 PUSHER PROPELLER

n (RPM)	F (LBF)	Q_{DMM} (mV)
4400	2.21	0.173
4700	2.22	0.191
5100	2.23	0.210
5600	2.26	0.263
6200	2.29	0.320
6900	2.33	0.392
7700	2.39	0.502
8500	2.45	0.611

START TARE 2.11
END TARE 2.12

DATE: 02-24-89

l = 21.93 IN

TABLE V

ELECTRIC MOTOR TORQUE STAND RAW DATA

		10 X 7		11 X 8		14 X 8	
THROTTLE (PERCENT)	VOLTAGE (VOLTS)	n (RPM)	F (LBF)	n (RPM)	F (LBF)	n (RPM)	F (LBF)
20	36	3670	2.15	3230	2.15	2280	2.16
30	49	5150	2.16	4525	2.17	3390	2.18
40	62	6425	2.18	5720	2.19	4425	2.22
50	75	7665	2.20	6870	2.22	5365	2.26
60	88	8830	2.22	8000	2.26	6240	2.31
70	101	9890	2.24	8850	2.29	7015	2.37
80	114	10880	2.27	9830	2.31	7760	2.41
90	127	11700	2.30	10550	2.34	8240	2.45
100	140	-----	----	11080	2.38	8600	2.50
START TARE			2.12		2.12		2.12
STOP TARE			2.12		2.12		2.12

		16 X 8		18 X 8		20 X 8	
THROTTLE (PERCENT)	VOLTAGE (VOLTS)	n (RPM)	F (LBF)	n (RPM)	F (LBF)	n (RPM)	F (LBF)
20	36	1720	2.16	1490	2.16	1365	2.16
30	49	2715	2.19	2325	2.19	2140	2.20
40	62	3630	2.25	3135	2.26	2875	2.26
50	75	4425	2.29	3825	2.32	3520	2.33
60	88	5175	2.36	4455	2.38	4065	2.40
70	101	5920	2.42	5100	2.45	4650	2.46
80	114	6460	2.48	5560	2.52	4900	2.54
90	127	6860	2.53	5605	2.59	5100	2.60
100	140	7000	2.59	6000	2.64	5400	2.65
START TARE			2.12		2.13		2.13
STOP TARE			2.13		2.13		2.13

DATE: 02-24-89

l = 22.93 IN

TABLE VI

HALF-SCALE PIONEER ENGINE TORQUE STAND RAW DATA

THROTTLE (PERCENT)	DETENT	12 X 9 n (RPM)	12 X 9 F (LBF)	14 X 6 n (RPM)	14 X 6 F (LBF)	14 X 8 n (RPM)	14 X 8 F (LBF)
20	8	7630	2.23	6990	2.25	6730	2.26
30	10	9060	2.30	8500	2.31	7810	2.18
40	12	9870	2.34	9200	2.37	8600	2.39
50	14	10560	2.38	9540	2.41	9080	2.42
60	16	10890	2.39	9820	2.43	9450	2.44
70	18	11050	2.40	9910	2.44	9600	2.45
80	20	11110	2.41	9940	2.45	9650	2.46
90	22	11140	2.42	10030	2.45	9680	2.46
100	24	11160	2.42	10020	2.46	9630	2.53
START TARE			2.01		2.01		2.01
STOP TARE			2.02		2.01		2.01

THROTTLE (PERCENT)	DETENT	16 X 8 n (RPM)	16 X 8 F (LBF)	18 X 8 n (RPM)	18 X 8 F (LBF)
20	8	5660	2.30	4700	2.35
30	10	6480	2.39	5730	2.43
40	12	7000	2.45	6070	2.49
50	14	7300	2.47	6280	2.52
60	16	7450	2.49	6370	2.54
70	18	7490	2.50	6410	2.55
80	20	7500	2.50	6430	2.56
90	22	7620	2.51	6450	2.56
100	24	7640	2.53	6500	2.58
START TARE			2.01		2.01
STOP TARE			2.01		2.01

DATE: 02-25-89
TEMPERATURE: 66 F
PRESSURE: 30.10 IN HG
PP_{WV}: 0.13 IN HG

TABLE VII

WIND TUNNEL RAW DATA

n (RPM)	MOTOR VOLTAGE (VOLTS DC)	R_{DMM} (LBF)	D (LBF)
4400	42.28	-0.95	-1.10
4500	44.80	-1.05	-1.30
4700	49.84	-0.65	-1.10
4900	54.60	-0.50	-1.30
5100	59.22	-0.20	-1.10
5400	65.66	0.10	-1.30
5600	69.86	0.55	-1.10
5800	73.92	0.70	-1.30
6200	81.76	1.50	-1.10
6500	87.64	1.90	-1.30
6900	95.48	2.90	-1.10
7400	105.84	3.65	-1.30
7700	112.56	4.50	-1.10
8100	122.08	5.20	-1.30
8300	127.12	5.55	-1.30
8500	132.58	6.30	-1.10

DATE: 01-20-89
TEMPERATURE: 66.5 F
PRESSURE: 30.17 In Hg

TABLE VIII

FLIGHT TEST RAW DATA

RUN	THROTTLE SETTING (PERCENT)	TIME (SECS)	FREQUENCY (HZ)
A	100	9.81	344.3
B	100	10.22	354.4
A	95	9.62	349.1
B	95	10.47	352.2
A	90	9.75	340.1
B	90	10.37	348.2
A	85	9.93	340.8
B	85	10.22	335.9
A	80	9.81	338.7
B	80	10.41	341.3
A	75	9.91	334.5
B	75	10.42	336.8
A	70	10.00	336.2
B	70	10.45	337.8
A	65	9.65	340.4
B	65	10.94	329.6
A	60	9.82	336.2
B	60	10.86	330.1
A	55	10.27	339.3
B	55	10.42	325.7
A	50	10.45	330.1
B	50	10.68	333.9
A	45	10.60	336.1
B	45	10.81	327.2
A	40	10.72	337.6
B	40	11.60	317.7
A	35	12.50	319.8
B	35	12.69	315.2
A	30	15.23	252.5
B	30	15.36	247.5
A	25	15.35	241.5
B	25	17.73	235.1

DATE: 2-11-89
TEMPERATURE: 51.0 F
PRESSURE: 30.32 IN HG
DISTANCE: 1000 FT

APPENDIX D

SMOOTH DATA

TABLE I

ELECTRIC MOTOR TORQUE STAND POWER DATA

THROTTLE (PERCENT)	10 X 7 n (RPM)	10 X 7 SBHP (HP)	11 X 8 n (RPM)	11 X 8 SBHP (HP)	14 X 8 n (RPM)	14 X 8 SBHP (HP)
20	3670	0.041	3230	0.036	2280	0.025
30	5150	0.075	4525	0.082	3390	0.073
40	6425	0.139	5720	0.143	4425	0.157
50	7665	0.219	6870	0.224	5365	0.265
60	8830	0.313	8000	0.395	6240	0.417
70	9890	0.420	8850	0.530	7015	0.615
80	10880	0.576	9830	0.657	7760	0.789
90	11700	0.741	10550	0.815	8240	0.952
100	-----	----	11080	1.010	8600	1.143

THROTTLE (PERCENT)	16 X 8 n (RPM)	16 X 8 SBHP (HP)	18 X 8 n (RPM)	18 X 8 SBHP (HP)	20 X 8 n (RPM)	20 X 8 SBHP (HP)
20	1720	0.022	1490	0.017	1365	0.015
30	2715	0.063	2325	0.050	2140	0.054
40	3630	0.160	3135	0.144	2875	0.132
50	4425	0.257	3825	0.256	3520	0.247
60	5175	0.427	4455	0.391	4065	0.385
70	5920	0.612	5100	0.571	4650	0.537
80	6460	0.803	5560	0.758	4900	0.703
90	6860	0.972	5605	0.901	5100	0.838
100	7000	1.140	6000	1.070	5400	0.981

TABLE II

HALF-SCALE PIONEER ENGINE POWER DATA

	12 X 9		14 X 6		14 X 8	
THROTTLE (PERCENT)	n (RPM)	SBHP (HP)	n (RPM)	SBHP (HP)	n (RPM)	SBHP (HP)
20	7630	0.587	6990	0.586	6730	0.588
30	9060	0.918	8500	0.891	7810	0.873
40	9870	1.138	9200	1.158	8600	1.142
50	10560	1.366	9540	1.333	9080	1.301
60	10890	1.446	9820	1.441	9450	1.420
70	11050	1.506	9910	1.489	9600	1.476
80	11110	1.553	9990	1.536	9650	1.518
90	11140	1.596	10030	1.542	9680	1.522
100	11160	1.599	10020	1.576	9630	1.548

	16 X 8		18 X 8	
THROTTLE (PERCENT)	n (RPM)	SBHP (HP)	n (RPM)	SBHP (HP)
20	5660	0.574	5660	0.558
30	6480	0.861	5730	0.841
40	7000	1.076	6070	1.018
50	7300	1.174	6280	0.119
60	7450	1.250	6370	1.180
70	7490	1.283	6410	1.210
80	7500	1.284	6430	1.236
90	7620	1.332	6450	1.240
100	7640	1.388	6500	1.295

TABLE III

WIND TUNNEL DATA

n (RPM)	J	R_{DMM} (LBF)	Q (FT-LBS)	Q_{DMM} (mV X 10^2)	R (LBF)	D (LBF)	T_E (LBF)	C_T
4400	0.612	-0.95	0.170	0.030	-0.980	-1.10	0.120	0.0051
4500	0.657	-1.05	0.176	0.031	-1.081	-1.30	0.219	0.0089
4700	0.629	-0.65	0.188	0.033	-0.683	-1.10	0.417	0.0155
4900	0.603	-0.50	0.201	0.035	-0.535	-1.30	0.764	0.0261
5100	0.580	-0.20	0.216	0.038	-0.238	-1.10	0.862	0.0272
5400	0.547	0.10	0.240	0.042	0.058	-1.30	1.358	0.0383
5600	0.528	0.55	0.257	0.045	0.505	-1.10	1.605	0.0421
5800	0.510	0.70	0.276	0.048	0.652	-1.30	1.952	0.0477
6200	0.477	1.50	0.316	0.055	1.445	-1.10	2.545	0.0544
6500	0.455	1.90	0.349	0.061	1.839	-1.30	3.139	0.0610
6900	0.428	2.90	0.395	0.069	2.831	-1.10	3.931	0.0678
7400	0.399	3.65	0.458	0.080	3.570	-1.30	4.870	0.0731
7700	0.384	4.50	0.498	0.087	4.413	-1.10	5.513	0.0764
8100	0.365	5.20	0.553	0.097	5.103	-1.30	6.403	0.0802
8300	0.356	5.55	0.581	0.102	5.448	-1.30	6.748	0.0805
8500	0.348	6.30	0.610	0.107	6.193	-1.10	7.293	0.0829

TABLE IV

PROPELLER EFFICIENCY DATA

n (RPM)	J	T_E (LBF)	SBHP (HP)	η (PERCENT)
4400	0.6177	0.120	0.083	15.11
4500	0.6568	0.219	0.096	23.84
4700	0.6289	0.417	0.124	35.14
4900	0.6032	0.764	0.152	52.58
5100	0.5795	0.862	0.179	50.32
5400	0.5473	1.358	0.231	61.37
5600	0.5278	1.605	0.255	65.77
5800	0.5096	1.952	0.308	66.22
6200	0.4767	2.545	0.403	65.82
6500	0.4547	3.139	0.479	68.48
6900	0.4284	3.931	0.590	69.62
7400	0.3994	4.870	0.714	71.27
7700	0.3839	5.513	0.800	72.01
8100	0.3649	6.403	0.910	73.52
8300	0.3561	6.748	0.971	72.62
8500	0.3477	7.293	1.055	72.58

TABLE V

FLIGHT TEST DATA

THROTTLE (PERCENT)	V_T (FT/S)	n (RPM)	W_T (LBS)	J	η (PERCENT)	$SBHP_{STD}$ (HP)	C_T	T (LBS)
25	60.77	7150	26.50	0.44	70.7	0.728	0.1233	4.139
30	65.38	7500	26.55	0.45	70.2	0.870	0.1131	4.391
35	79.40	9525	26.60	0.43	70.9	1.054	0.1328	7.604
40	89.74	9830	26.65	0.47	69.3	1.140	0.0952	6.967
45	93.42	9950	26.70	0.48	68.8	1.240	0.0862	6.836
50	94.66	9960	26.75	0.49	67.8	1.350	0.0804	6.542
55	96.67	9975	26.80	0.50	67.0	1.398	0.0736	6.249
60	96.96	9995	26.40	0.50	67.0	1.445	0.0735	6.274
65	97.52	10050	26.45	0.50	67.0	1.469	0.0734	6.343
70	97.84	10110	26.50	0.50	67.0	1.495	0.0738	6.419
75	98.44	10220	26.55	0.50	67.0	1.524	0.0745	6.560
80	99.00	10200	26.60	0.50	67.0	1.545	0.0734	6.534
85	99.28	10150	26.65	0.50	67.0	1.544	0.0732	6.470
90	99.50	10325	26.70	0.50	67.0	1.555	0.0744	6.695
95	99.73	10520	26.75	0.49	67.8	1.578	0.0807	7.298
100	99.89	10480	26.80	0.49	67.8	1.590	0.0799	7.243

TABLE VI

DRAG POLAR DATA
(POWER METHOD)

THROTTLE (PERCENT)	C_L	C_D
25	0.790	0.1430
30	0.684	0.1362
35	0.465	0.0931
40	0.364	0.0682
45	0.337	0.0653
50	0.329	0.0673
55	0.316	0.0646
60	0.309	0.0662
65	0.306	0.0661
70	0.305	0.0667
75	0.302	0.0668
80	0.299	0.0665
85	0.298	0.0659
90	0.297	0.0659
95	0.296	0.0672
100	0.296	0.0674

TABLE VII

POWER REQUIRED DATA
(POWER METHOD)

THROTTLE (PERCENT)	P_{i_w} (HP)	V_{i_w} (FT/S)
25	0.540	61.75
30	0.639	66.37
35	0.780	80.50
40	0.822	90.92
45	0.885	94.56
50	0.947	95.72
55	0.966	97.68
60	1.021	98.70
65	1.036	99.20
70	1.051	99.41
75	1.068	99.92
80	1.080	100.41
85	1.076	100.60
90	1.081	100.72
95	1.107	100.87
100	1.112	100.94

TABLE VIII

DRAG POLAR DATA
(THRUST METHOD)

THROTTLE (PERCENT)	C_L	C_D
25	0.790	0.1233
30	0.684	0.1131
35	0.465	0.1328
40	0.364	0.0952
45	0.337	0.0862
50	0.329	0.0804
55	0.316	0.0736
60	0.309	0.0735
65	0.306	0.0734
70	0.305	0.0738
75	0.302	0.0645
80	0.299	0.0734
85	0.298	0.0722
90	0.297	0.0744
95	0.296	0.0807
100	0.296	0.0799

TABLE IX

POWER REQUIRED DATA
(THRUST METHOD)

THROTTLE (PERCENT)	P_{iw} (HP)	V_{iw} (FT/S)
25	0.480	61.75
30	0.537	66.37
35	1.145	80.50
40	1.176	90.92
45	1.204	94.56
50	1.217	95.72
55	1.133	97.68
60	1.167	98.70
65	1.183	99.20
70	1.198	99.41
75	1.229	99.92
80	1.227	100.41
85	1.215	100.60
90	1.256	100.72
95	1.369	100.87
100	1.357	100.94

LIST OF REFERENCES

1. Gwynne, P., "Remotely Piloted Vehicles Join the Service," High Technology, January 1987.

2. Thompson, M., "Contract Bypassed U.S. Rules," San Jose Mercury News, 24 July 1988.

3. Sestak, Timothy A., Measurement of the Aerodynamic Forces Generated by Flight Crew Helmets in Supercritical Subsonic Flow, Master's Thesis, Naval Postgraduate School, March 1987.

4. Sargaent, Christopher L., The Influence of Helicopter Tail Shape on Drag, an Aerodynamic Study Using a Low Speed Wind Tunnel, Master's Thesis, Naval Postgraduate School, March 1985.

5. Roberts, Sean C., Light Aircraft Performance for Test Pilots and Flight Test Engineers, Flight Research, Inc., 1982.

6. Sanders, Milton R., Propeller and Engine Testing for a Mini-Remote Piloted Vehicle, Master's Thesis, Air Force Technology, Wright-Patterson AFB, Ohio, March 1975.

7. Nelson, Wilbur C., Airplane Propeller Principles, John Wiley & Sons, Inc., 1944.

8. National Advisory Council on Aeronautics Technical Report No. 507, Tests of Nacelle-Propeller Combinations in Various Positions with Reference to Wings, by Donald H. Wood, and Carlton Bioletti, 1934.

9. Anderson, John D., Introduction to Flight, McGraw-Hill Book Company, 1985.

10. Naval Postgraduate School, Department of Aeronautics, Laboratory Manual for Low Speed Wind Tunnel Testing, Handout September 1987.

11. Beer, Ferdinand P., and Johnson, Russell, E., Jr., Mechanics of Materials, McGraw-Hill Book Company, 1981.

INITIAL DISTRIBUTION LIST

		No. Copies
1.	Defense Technical Information Center Cameron Station Alexandria, VA 22304-6145	2
2.	Library, Code 0142 Naval Postgraduate School Monterey, CA 93943-5002	2
3.	Chairman, Code 67 Department of Aeronautics and Astronautics Naval Postgraduate School Monterey, CA 93953-5000	2
4.	Professor R. M. Howard, Code 67 Ho Department of Aeronautics and Astronautics Naval Postgraduate School Monterey, CA 93953-5000	7
5.	Lt. Eric Pagenkopf, Code 67 Pa Department of Aeronautics and Astronautics Naval Postgraduate School Monterey, CA 93953-5000	1
6.	Lt. James C. Tanner 23540 Via Amado Valencia, CA 91355	2
7.	Howard Crispin Academy of Model Aeronautics 1810 Samuel Morse Drive Reston, VA 22090	1
8.	Mr. Harry Berman Naval Air Systems Command Aircraft Division--Research and Technology Air 931M Washington, DC 20360	1
9.	Mr. Rick J. Foch Naval Research Laboratory Code 5712 4555 Overlook Avenue, S.W. Washington, DC 20375	1

10. Commanding Officer 1
Unmanned Aerial Vehicles Joint Program Office
Naval Air Systems Command
PMA 263M
Washington, DC 20361-1263

11. Commanding Officer 1
UAV Test & Evaluation Office
ATTN: Maj. Paul Donohue
Pacific Missile Test Center
Pt. Mugu, CA 93042

Thesis
T1368
c.1

Tanner
Development of a flight test methodology for a U.S. Navy half-scale Unmanned Air Vehicle.